Preparations for quantum simulations of quantum chromodynamics in 1 + 1 dimensions. II. Single-baryon β-decay in real time

Roland C. Farrell,[1,*] Ivan A. Chernyshev,[1,†] Sarah J. M. Powell,[2,‡] Nikita A. Zemlevskiy,[1,§] Marc Illa,[1,‖] and Martin J. Savage[1,¶]

[1]*InQubator for Quantum Simulation (IQuS), Department of Physics, University of Washington, Seattle, Washington 98195, USA*

[2]*Department of Physics and Astronomy, York University, Toronto, Ontario M3J 1P3, Canada*

(Received 2 November 2022; accepted 17 February 2023; published 30 March 2023; corrected 18 April 2023)

A framework for quantum simulations of real-time weak decays of hadrons and nuclei in a two-flavor lattice theory in one spatial dimension is presented. A single generation of the Standard Model is found to require 16 qubits per spatial lattice site after mapping to spin operators via the Jordan-Wigner transformation. Both quantum chromodynamics and flavor-changing weak interactions are included in the dynamics, the latter through four-Fermi effective operators. Quantum circuits that implement time evolution in this lattice theory are developed and run on Quantinuum's `H1-1` 20-qubit trapped ion system to simulate the β-decay of a single baryon on one lattice site. These simulations include the initial state preparation and are performed for both one and two Trotter time steps. The potential intrinsic error-correction properties of this type of lattice theory are discussed, and the leading lattice Hamiltonian required to simulate $0\nu\beta\beta$-decay of nuclei induced by a neutrino Majorana mass term is provided.

DOI: 10.1103/PhysRevD.107.054513

I. INTRODUCTION

A quantitative exploration of hadronic decays and nuclear reaction dynamics resolved at very short timescales using quantum simulations will provide a new window into strong-interaction processes that lies beyond the capabilities of experiment. In chemistry, the development of femtosecond laser-pulse imaging in the 1980s [1] allowed for reaction pathways to be studied in real time (for an overview, see Ref. [2]). Although a similar experimental procedure is not available for strong processes, it is expected that quantum simulations will provide analogous insight into hadronic dynamics. Perhaps the simplest nontrivial class of such reactions to begin exploring is the β-decay of low-lying hadrons and nuclei. Single β-decay rates of nuclei have played a central role in defining the Standard Model (SM) of strong and electroweak processes [3–6]. They initially provided evidence that the weak (charged-current) quark eigenstates differ from the strong eigenstates and, more recently, are providing stringent tests of the unitarity of the Cabibbo-Kobayashi-Maskawa (CKM) matrix [7,8]. For recent reviews of β-decay, see, e.g., Refs. [9–12]. The four-Fermi operators responsible for β-decay [13] in the SM emerge from operator production expansions (OPEs) of the nonlocal operators coming from the exchange of a charged-gauge boson (W^-) between quarks and leptons. Of relevance to this work is the four-Fermi operator, which gives rise to the flavor changing quark process $d \to u e^- \bar{\nu}$. In the absence of higher-order electroweak processes, including electromagnetism, matrix elements of these operators factorize between the hadronic and leptonic sectors. This leaves, for example, a nonperturbative evaluation of $n \to p e^- \bar{\nu}$ for neutron decay, which is constrained significantly by the approximate global flavor symmetries of QCD. Only recently have the observed systematics of β-decay rates of nuclei been understood without the need for phenomenological rescalings of the axial coupling constant, g_A. As has long been anticipated, the correct decay rates are recovered when two-nucleon and higher-body interactions are included within the effective field theories (EFTs) (or meson-exchange currents) [14–17]. This was preceded by successes of EFTs in describing electroweak processes of few-nucleon systems through the inclusion of higher-body electroweak operators (not constrained by strong interactions alone), e.g., Refs. [18–23]. The EFT framework describing nuclear β-decays involves contributions from "potential-pion" and "radiation-pion" exchanges [24,25] (an artifact of a system of relativistic and nonrelativistic particles [26,27]), and real-time simulations of these processes are expected to be able to isolate these distinct contributions.

*Corresponding author.
rolanf2@uw.edu
†ivanc3@uw.edu
‡spow9@uw.edu
§zemlni@uw.edu
‖marcilla@uw.edu
¶mjs5@uw.edu

Recently, the first Euclidean-space lattice QCD calculations of Gamow-Teller matrix elements in light nuclei (at unphysical light quark masses and without fully quantified uncertainties) have been performed [28], finding results that are consistent with nature.

While β-decay is a well-studied and foundational area of subatomic physics, the double-β-decay of nuclei continues to present a theoretical challenge in the search for physics beyond the SM. For a recent review of the "status and prospects" of $\beta\beta$-decay, see Ref. [29]. Although $2\nu\beta\beta$-decay is allowed in the SM and is a second order β-decay process, $0\nu\beta\beta$-decay requires the violation of lepton number. Strong interactions clearly play an essential role in the experimental detection of the $\beta\beta$-decay of nuclei, but such contributions are nonperturbative and complex, and, for example, the EFT descriptions involve contributions from two- and higher-body correlated operators [30–34]. The ability to study the real-time dynamics of such a decay process in nuclei would likely provide valuable insight into the underlying strong-interaction mechanisms, and potentially offer first principles constraints beyond those from Euclidean-space lattice QCD.[1]

Significant progress is being made toward quantum simulations of quantum field theories, both conceptually and using NISQ quantum simulators and devices [41–167]. Simulations of systems of quarks and gluons with $L = 1, 2$ spatial sites in one dimension and one or two plaquettes of Yang-Mills gauge theories are now being performed on quantum devices [80,105,109,138,142,155,158,159]. The spatial and temporal extent of such simulations are steadily increasing as both error-mitigation strategies and device performance improve. There has also been important algorithmic development on how decay widths and cross sections can be extracted from the computation of Green functions on quantum hardware [168]. Recently, results of classical and quantum simulations of $SU(3)$ gauge theory with $N_f = 1, 2$ flavors of quarks in $1 + 1$ dimensions were presented [158,159]. With a layout footprint of six qubits per flavor per lattice site using the Jordan-Wigner (JW) mapping [169], one Trotter step of time evolution of one spatial site was simulated using IBM's superconducting quantum computers [170], obtaining uncertainties at the percent level.

This paper extends our recent work [158] to include flavor-changing weak interactions via a four-Fermi operator that generates the β-decay of hadrons and nuclei. The terms in the lattice Hamiltonian that generate a Majorana mass for the neutrinos are also given, although not included in the simulations. Applying the JW mapping, it is found that a single generation of the SM (quarks and leptons) maps onto 16 qubits per spatial lattice site. Using Quantinuum's `H1-1` 20-qubit trapped-ion quantum computer, the initial state of a baryon is both prepared and evolved with one and two Trotter steps on a single lattice site. Despite only employing a minimal amount of error mitigation, results at the $\sim$5%-level are obtained, consistent with the expectations. Finally, we briefly comment on the potential of such hierarchical dynamics for error-correction purposes in quantum simulations.

[1]For discussions of the potential of lattice QCD to impact $\beta\beta$-decay, see, e.g., Refs. [31,32,35–40].

II. THE β-DECAY HAMILTONIAN FOR QUANTUM SIMULATIONS IN 1 + 1 DIMENSIONS

In nature, the β-decays of neutrons and nuclei involve energy and momentum transfers related to the energy scales of nuclear forces and of isospin breaking. As these are much below the electroweak scale, β-decay rates are well reproduced by matrix elements of four-Fermi effective interactions with $V - A$ structure [13,171], of the form

$$\mathcal{H}_\beta = \frac{G_F}{\sqrt{2}} V_{ud} \bar{\psi}_u \gamma^\mu (1-\gamma_5) \psi_d \bar{\psi}_e \gamma_\mu (1-\gamma_5) \psi_{\nu_e} + \text{H.c.}, \quad (1)$$

where V_{ud} is the element of the CKM matrix for $d \to u$ transitions, and G_F is Fermi's coupling constant that is measured to be $G_F = 1.1663787(6) \times 10^{-5}$ GeV^{-2} [172]. This is the leading order (LO) SM result, obtained by matching amplitudes at tree level, where $G_F/\sqrt{2} = g_2^2/(8M_W^2)$, with M_W the mass of the $W^\pm$ gauge boson and g_2 the SU$(2)_L$ coupling constant. Toward simulating the SM in 3 + 1D, we consider 1 + 1D QCD containing u quarks, d quarks, electrons, and electron neutrinos. For simplicity, we model β-decay through a vectorlike four-Fermi operator,

$$\mathcal{H}_\beta^{1+1} = \frac{G}{\sqrt{2}} \bar{\psi}_u \gamma^\mu \psi_d \bar{\psi}_e \gamma_\mu \mathcal{C} \psi_\nu + \text{H.c.}, \quad (2)$$

where $\mathcal{C} = \gamma_1$ is the charge-conjugation operator whose purpose will become clear. Appendices B and C provide details on calculating the single-baryon β-decay rates in the infinite volume and continuum limits in the SM and in the 1 + 1D model considered here.

The strong and weak interactions can be mapped onto the finite-dimensional Hilbert space provided by a quantum computer by using the Kogut-Susskind (KS) Hamiltonian formulation of lattice gauge theory [173,174]. The KS discretization of the fields is such that L spatial lattice sites are split into $2L$ fermion sites that separately accommodate fermions (even sites) and antifermions (odd sites). For the β-decay of baryons, the strong and the weak KS Hamiltonian (in axial gauge) has the form [64,109,158,159]

$$H = H_{\text{quarks}} + H_{\text{leptons}} + H_{\text{glue}} + H_\beta, \quad (3)$$

where

$$
\begin{aligned}
H_{\text{quarks}} &= \sum_{f=u,d}\left[\frac{1}{2a}\sum_{n=0}^{2L-2}(\phi_n^{(f)\dagger}\phi_{n+1}^{(f)}+\text{H.c.})+m_f\sum_{n=0}^{2L-1}(-1)^n\phi_n^{(f)\dagger}\phi_n^{(f)}\right],\\
H_{\text{leptons}} &= \sum_{f=e,\nu}\left[\frac{1}{2a}\sum_{n=0}^{2L-2}(\chi_n^{(f)\dagger}\chi_{n+1}^{(f)}+\text{H.c.})+m_f\sum_{n=0}^{2L-1}(-1)^n\chi_n^{(f)\dagger}\chi_n^{(f)}\right],\\
H_{\text{glue}} &= \frac{ag^2}{2}\sum_{n=0}^{2L-2}\sum_{a=1}^{8}\left(\sum_{m\le n}Q_m^{(a)}\right)^2,\\
H_\beta &= \frac{G}{a\sqrt{2}}\sum_{l=0}^{L-1}[(\phi_{2l}^{(u)\dagger}\phi_{2l}^{(d)}+\phi_{2l+1}^{(u)\dagger}\phi_{2l+1}^{(d)})(\chi_{2l}^{(e)\dagger}\chi_{2l+1}^{(\nu)}-\chi_{2l+1}^{(e)\dagger}\chi_{2l}^{(\nu)})\\
&\quad+(\phi_{2l}^{(u)\dagger}\phi_{2l+1}^{(d)}+\phi_{2l+1}^{(u)\dagger}\phi_{2l}^{(d)})(\chi_{2l}^{(e)\dagger}\chi_{2l}^{(\nu)}-\chi_{2l+1}^{(e)\dagger}\chi_{2l+1}^{(\nu)})+\text{H.c.}].
\end{aligned}
\tag{4}
$$

The masses of the u, d quarks, electron, and neutrino (Dirac) are $m_{u,d,e,\nu}$, and the strong and weak coupling constants are g and G. The $SU(3)$ charges are $Q_m^{(a)}$, and $\phi_n^{(u,d)}$ are the u- and d-quark field operators (which both transform in the fundamental representation of $SU(3)$, and hence, the sum over color indices has been suppressed). The electron and neutrino field operators are $\chi_n^{(e,\nu)}$, and for the remainder of this paper, the lattice spacing, a, will be set to unity. We emphasize that the absence of gluon fields is due to the choice of axial gauge, whereas the lack of weak gauge fields is due to the consideration of a low energy effective theory in which the heavy weak gauge bosons have been integrated out. This results in, for example, the absence of parallel transporters in the fermion kinetic terms.

The JW mapping of the Hamiltonian in Eq. (4) to qubits, arranged as shown in Fig. 1, is given by

$$
\begin{aligned}
H_{\text{quarks}} &\to \frac{1}{2}\sum_{l=0}^{L-1}\sum_{f=u,d}\sum_{c=0}^{2}m_f(Z_{l,f,c}-Z_{l,\bar{f},c}+2)\\
&\quad-\frac{1}{2}\sum_{l=0}^{L-1}\sum_{f=u,d}\sum_{c=0}^{2}[\sigma_{l,f,c}^{+}Z^7\sigma_{l,\bar{f},c}^{-}+(1-\delta_{l,L-1})\sigma_{l,\bar{f},c}^{+}Z^7\sigma_{l+1,f,c}^{-}+\text{H.c.}],\\
H_{\text{leptons}} &\to \frac{1}{2}\sum_{l=0}^{L-1}\sum_{f=e,\nu}m_f(Z_{l,f}-Z_{l,\bar{f}}+2)-\frac{1}{2}\sum_{l=0}^{L-1}\sum_{f=e,\nu}[\sigma_{l,f}^{+}Z^7\sigma_{l,\bar{f}}^{-}+(1-\delta_{l,L-1})\sigma_{l,\bar{f}}^{+}Z^7\sigma_{l+1,f}^{-}+\text{H.c.}],\\
H_{\text{glue}} &\to \frac{g^2}{2}\sum_{n=0}^{2L-2}(2L-1-n)\left(\sum_{f=u,d}Q_{n,f}^{(a)}Q_{n,f}^{(a)}+2Q_{n,u}^{(a)}Q_{n,d}^{(a)}\right)+g^2\sum_{n=0}^{2L-3}\sum_{m=n+1}^{2L-2}(2L-1-m)\sum_{f=u,d}\sum_{f'=u,d}Q_{n,f}^{(a)}Q_{m,f'}^{(a)},\\
H_\beta &\to \frac{G}{\sqrt{2}}\sum_{l=0}^{L-1}\sum_{c=0}^{2}(\sigma_{l,\bar{\nu}}^{-}Z^6\sigma_{l,e}^{+}\sigma_{l,d,c}^{-}Z^2\sigma_{l,u,c}^{+}-\sigma_{l,\bar{e}}^{+}Z^8\sigma_{l,\nu}^{-}\sigma_{l,d,c}^{-}Z^2\sigma_{l,u,c}^{+}-\sigma_{l,\bar{\nu}}^{-}Z^{2-c}\sigma_{l,\bar{d},c}^{-}\sigma_{l,\bar{u},c}^{+}Z^c\sigma_{l,e}^{+}\\
&\quad+\sigma_{l,\bar{e}}^{+}Z^{3-c}\sigma_{l,\bar{d},c}^{-}\sigma_{l,\bar{u},c}^{+}Z^{1+c}\sigma_{l,\nu}^{-}-\sigma_{l,\bar{d},c}^{-}Z^{3+c}\sigma_{l,e}^{+}\sigma_{l,\nu}^{-}Z^{5-c}\sigma_{l,u,c}^{+}-\sigma_{l,\bar{e}}^{+}\sigma_{l,\bar{\nu}}^{-}\sigma_{l,\bar{d},c}^{-}Z^{10}\sigma_{l,u,c}^{+}\\
&\quad-\sigma_{l,\bar{u},c}^{+}Z^c\sigma_{l,e}^{+}\sigma_{l,\nu}^{-}Z^{2-c}\sigma_{l,d,c}^{-}-\sigma_{l,\bar{e}}^{+}\sigma_{l,\bar{\nu}}^{-}\sigma_{l,\bar{u},c}^{+}Z^4\sigma_{l,d,c}^{-}+\text{H.c.}),
\end{aligned}
\tag{5}
$$

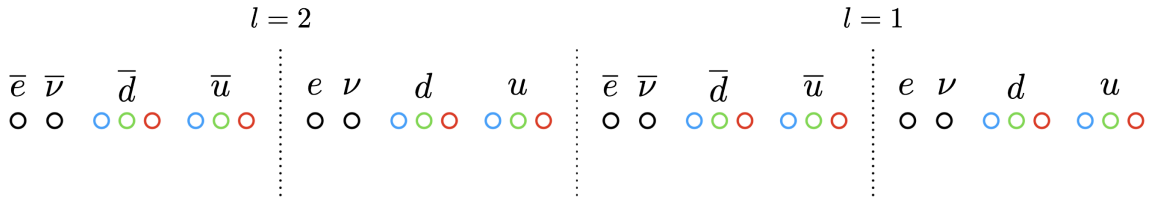

FIG. 1. The qubit layout of a $L = 2$ lattice, where fermions and antifermions are grouped together (which will be preferred if electromagnetism is included). This layout extends straightforwardly to $L > 2$.

where the sums of products of color charges are

$$Q^{(a)}_{n,f}Q^{(a)}_{n,f} = 1 - \frac{1}{3}\sum_{c=0}^{1}\sum_{c'>c} Z_{n,f,c}Z_{n,f,c'},$$
$$Q^{(a)}_{n,f}Q^{(a)}_{m,f'} = \frac{1}{2}\sum_{c=0}^{1}\sum_{c'>c}(\sigma^{+}_{n,f,c}Z^{c'-c-1}\sigma^{-}_{n,f,c'}\sigma^{-}_{m,f',c}Z^{c'-c-1}\sigma^{+}_{m,f',c'} + \text{H.c.}) + \frac{1}{24}\sum_{c=0}^{2}\sum_{c'=0}^{2}(3\delta_{cc'}-1)Z_{n,f,c}Z_{m,f',c'}, \quad (6)$$

and the repeated $SU(3)$ adjoint indices, $a = 1, 2, \ldots, 8$, are summed over. The index l labels the spatial lattice site, $f(\bar{f})$ labels the (anti)fermion flavor, and $c = 0, 1, 2$ corresponds to red, green, and blue colors. In the staggered mapping, there are gauge-field links every half of a spatial site and, as a result, the color charges are labeled by a half site index, n. The spin raising and lowering operators are $\sigma^{\pm} = \frac{1}{2}(\sigma^x \pm i\sigma^y)$, $Z = \sigma^z$, and unlabeled Zs act on the sites between the $\sigma^{\pm}$, e.g., $\sigma^{-}_{l,d,r}Z^2\sigma^{+}_{l,u,r} = \sigma^{-}_{l,d,r}Z_{l,u,b}Z_{l,u,g}\sigma^{+}_{l,u,r}$. Constants have been added to the mass terms to ensure that all basis states contribute positive mass.

A. Efficiently mapping the $L = 1$ Hamiltonian to qubits

To accommodate the capabilities of current devices, the quantum simulations performed in this work involve only a single spatial site, $L = 1$, where the structure of the Hamiltonian can be simplified. In particular, without interactions between leptons, it is convenient to work with field operators that create and annihilate eigenstates of the free lepton Hamiltonian, H_{leptons}. These are denoted by "tilde operators" [158], which create the open-boundary-condition (OBC) analogs of plane waves. In the tilde basis with the JW mapping, the lepton Hamiltonian is diagonal and becomes

$$\tilde{H}_{\text{leptons}} = \lambda_\nu(\tilde{\chi}^{(\nu)\dagger}_0\tilde{\chi}^{(\nu)}_0 - \tilde{\chi}^{(\nu)\dagger}_1\tilde{\chi}^{(\nu)}_1) + \lambda_e(\tilde{\chi}^{(e)\dagger}_0\tilde{\chi}^{(e)}_0 - \tilde{\chi}^{(e)\dagger}_1\tilde{\chi}^{(e)}_1)$$
$$\to \frac{\lambda_\nu}{2}(Z_\nu - Z_{\bar{\nu}}) + \frac{\lambda_e}{2}(Z_e - Z_{\bar{e}}), \quad (7)$$

where $\lambda_{\nu,e} = \frac{1}{2}\sqrt{1 + 4m^2_{\nu,e}}$. The β-decay operator in Eq. (4) becomes

$$\tilde{H}_\beta = \frac{G}{\sqrt{2}}\Big\{(\phi^{(u)\dagger}_0\phi^{(d)}_0 + \phi^{(u)\dagger}_1\phi^{(d)}_1)\Big[\frac{1}{2}(s^e_+s^\nu_- - s^e_-s^\nu_+)(\tilde{\chi}^{(e)\dagger}_0\tilde{\chi}^{(\nu)}_0 + \tilde{\chi}^{(e)\dagger}_1\tilde{\chi}^{(\nu)}_1) + \frac{1}{2}(s^e_+s^\nu_+ + s^e_-s^\nu_-)(\tilde{\chi}^{(e)\dagger}_0\tilde{\chi}^{(\nu)}_1 - \tilde{\chi}^{(e)\dagger}_1\tilde{\chi}^{(\nu)}_0)\Big]$$
$$+ (\phi^{(u)\dagger}_0\phi^{(d)}_1 + \phi^{(u)\dagger}_1\phi^{(d)}_0)\Big[\frac{1}{2}(s^e_+s^\nu_+ - s^e_-s^\nu_-)(\tilde{\chi}^{(e)\dagger}_0\tilde{\chi}^{(\nu)}_0 - \tilde{\chi}^{(e)\dagger}_1\tilde{\chi}^{(\nu)}_1) - \frac{1}{2}(s^e_+s^\nu_- + s^e_-s^\nu_+)(\tilde{\chi}^{(e)\dagger}_0\tilde{\chi}^{(\nu)}_1 + \tilde{\chi}^{(e)\dagger}_1\tilde{\chi}^{(\nu)}_0)\Big] + \text{H.c.}\Big\}, \quad (8)$$

where $s^{\nu,e}_\pm = \sqrt{1 \pm m_{\nu,e}/\lambda_{\nu,e}}$. In our simulations, the initial state of the quark-lepton system is prepared in a strong eigenstate with baryon number $B = +1$ in the quark sector and the vacuum, $|\Omega\rangle_{\text{lepton}}$, in the lepton sector. One of the benefits of working in the tilde basis is that the vacuum satisfies $\tilde{\chi}^{(e,\nu)}_0|\Omega\rangle_{\text{lepton}} = \tilde{\chi}^{(e,\nu)\dagger}_1|\Omega\rangle_{\text{lepton}} = 0$, and the first and third terms of Eq. (8) do not contribute to β-decay. For the processes we are interested in, this results in an effective β-decay operator of the form

$$\tilde{H}_\beta = \frac{G}{\sqrt{2}}\Big\{(\phi^{(u)\dagger}_0\phi^{(d)}_0 + \phi^{(u)\dagger}_1\phi^{(d)}_1)\Big[\frac{1}{2}(s^e_+s^\nu_+ + s^e_-s^\nu_-)(\tilde{\chi}^{(e)\dagger}_0\tilde{\chi}^{(\nu)}_1 - \tilde{\chi}^{(e)\dagger}_1\tilde{\chi}^{(\nu)}_0)\Big]$$
$$- (\phi^{(u)\dagger}_0\phi^{(d)}_1 + \phi^{(u)\dagger}_1\phi^{(d)}_0)\Big[\frac{1}{2}(s^e_+s^\nu_- + s^e_-s^\nu_+)(\tilde{\chi}^{(e)\dagger}_0\tilde{\chi}^{(\nu)}_1 + \tilde{\chi}^{(e)\dagger}_1\tilde{\chi}^{(\nu)}_0)\Big] + \text{H.c.}\Big\}. \quad (9)$$

The insertion of the charge-conjugation matrix, $\mathcal{C}$, in the continuum operator, Eq. (2), is necessary to obtain a β-decay operator that does not annihilate the lepton vacuum. To minimize the length of the string of Zs in the JW mapping, the lattice layout in Fig. 2 is used. In this layout, the hopping piece of H_{quarks} has only five Zs between the quark and antiquark raising and lowering operators, and the β-decay operator is

$$\tilde{H}_\beta \to \frac{G}{\sqrt{2}}\sum_{c=r,g,b}\Big[\frac{1}{2}(s^e_+s^\nu_+ + s^e_-s^\nu_-)(\sigma^-_{\bar{\nu}}\sigma^+_e - \sigma^+_{\bar{e}}Z^2\sigma^-_\nu)(\sigma^-_{\bar{d},c}Z^2\sigma^+_{u,c} + \sigma^-_{\bar{d},c}Z^2\sigma^+_{\bar{u},c})$$
$$- \frac{1}{2}(s^e_+s^\nu_- + s^e_-s^\nu_+)(\sigma^-_{\bar{\nu}}\sigma^+_e + \sigma^+_{\bar{e}}Z^2\sigma^-_\nu)(\sigma^-_{\bar{d},c}Z^8\sigma^+_{u,c} + \sigma^+_{\bar{u},c}Z^2\sigma^-_{d,c}) + \text{H.c.}\Big]. \quad (10)$$

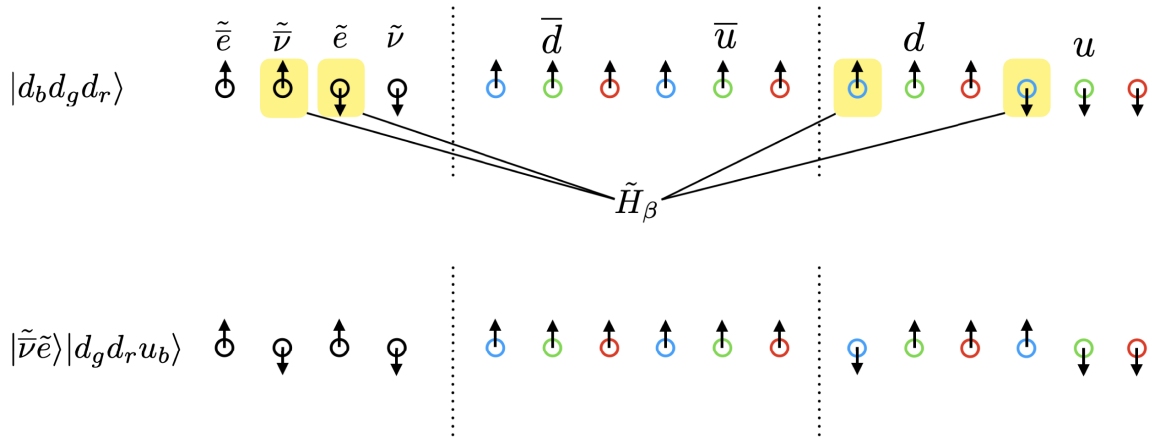

FIG. 2. The $L = 1$ lattice qubit layout of one generation of the SM that is used in this paper for quantum simulation. Fermion (antifermion) sites are occupied when the spin is up (down), and the spins at the lepton sites represent occupation in the tilde basis. Specifically, the example of $|d_b d_g d_r\rangle$ (upper lattice) decaying to $|\tilde{\nu}\,\tilde{e}\rangle|d_g d_r u_b\rangle$ (lower lattice) through one application of $\tilde{H}_\beta$ in Eq. (10) is shown.

In total, the $L = 1$ system requires 16 (12 quark and 4 lepton) qubits. See Appendix A for the complete $L = 1$ Hamiltonian in terms of qubits.

B. A Majorana mass for the neutrino

Although not relevant to the simulations performed in Sec. III, it is of current interest to consider the inclusion of a Majorana mass term for the neutrinos. A Majorana mass requires and induces the violation of lepton number by $|\Delta L| = 2$, and is not present in the minimal SM, defined by dimension-four operators. However, the Weinberg operator [175] enters at dimension-five and generates an effective Majorana mass for the neutrinos,

$$\mathcal{L}^{\text{Weinberg}} = \frac{1}{2\Lambda}(\bar{L}^c \epsilon\phi)(\phi^T \epsilon L) + \text{H.c.}, \qquad L = (\nu, e)^T_L, \qquad \phi = (\phi^+, \phi^0)^T, \qquad \langle\phi\rangle = (0, v/\sqrt{2})^T, \qquad \epsilon = i\sigma_2,$$
$$\to -\frac{v^2}{4\Lambda}\bar{\nu}^c_L \nu_L + \text{H.c.} + \cdots. \tag{11}$$

where ϕ is the Higgs doublet, L^c denotes the charge-conjugated left-handed lepton doublet, v is the Higgs vacuum expectation value, and Λ is a high-energy scale characterizing physics beyond the SM. The ellipsis denote interaction terms involving components of the Higgs doublet fields and the leptons. This is the leading contribution beyond the minimal SM but does not preclude contributions from other sources. On a $1 + 1$D lattice, there is only a single $|\Delta L| = 2$ local operator with the structure of a mass term and, using the JW mapping along with qubit layout in Fig. 1

$$H_{\text{Majorana}} = \frac{1}{2} m_M \sum_{n=\text{even}}^{2L-2} (\chi^{(\nu)}_n \chi^{(\nu)}_{n+1} + \text{H.c.})$$
$$\to \frac{1}{2} m_M \sum_{l=0}^{L-1} (\sigma^+_{l,\nu} Z^7 \sigma^+_{l,\bar{\nu}} + \text{H.c.}). \tag{12}$$

While the operator has support on a single spatial lattice site, it does not contribute to $0\nu\beta\beta$-decay on a lattice with only a single spatial site. This is because the processes that it could potentially induce, such as $\Delta^-\Delta^- \to \Delta^0\Delta^0 e^- e^-$, are Pauli blocked by the single electron site. At least two spatial sites are required for any such process producing two electrons in the final state.

III. QUANTUM SIMULATIONS OF THE β-DECAY OF ONE BARYON ON ONE LATTICE SITE

In this section, quantum simulations of the β-decay of a single baryon are performed in $N_f = 2$ flavor QCD with $L = 1$ spatial lattice site. The required quantum circuits to perform one and two Trotter steps of time evolution were developed and run on the Quantinuum `H1-1` 20 qubit

trapped ion quantum computer and its simulator `H1-1E` [176,177].

A. Preparing to simulate β-decay

It is well known that, because of confinement, the energy eigenstates (asymptotic states) of QCD are color-singlet hadrons, which are composite objects of quarks and gluons. On the other hand, the operators responsible for β-decay, given in Eq. (10), generate transitions between d and u quarks. As a result, observable effects of $\tilde{H}_\beta$, in part, are found in transitions between hadronic states whose matrix elements depend on the distribution of the quarks within. Toward quantum simulations of the β-decay of neutrons and nuclei more generally, the present work focuses on the decay of a single baryon.

Generically, three elements are required for real-time quantum simulations of the β-decay of baryons:

(1) Prepare the initial hadronic state that will subsequently undergo β-decay. In this work, this is one of the single-baryon states (appropriately selected in the spectrum) that is an eigenstate of the strong Hamiltonian alone; i.e., the weak coupling constant is set equal to $G = 0$.
(2) Perform (Trotterized) time evolution using the full ($G \neq 0$) Hamiltonian.
(3) Measure one or more of the lepton qubits. If leptons are detected, then β-decay has occurred.

In $1+1$D, Fermi statistics preclude the existence of a light isospin $I = 1/2$ nucleon, and the lightest baryons are in an $I = 3/2$ multiplet $(\Delta^{++}, \Delta^{+}, \Delta^{0}, \Delta^{-})$ (using the standard electric charge assignments of the up and down quarks). We have chosen to simulate the decay $\Delta^- \to \Delta^0 + e + \bar{\nu}$, which, at the quark level, involves baryon-interpolating operators with the quantum numbers of $ddd \to udd$.

In order for β-decay to be kinematically allowed, the input-parameters of the theory must be such that $M_{\Delta^-} > M_{\Delta^0} + M_{\bar{\nu}} + M_e$. This is accomplished through tuning the parameters of the Hamiltonian. The degeneracy in the iso-multiplet is lifted by using different values for the up and down quark masses. It is found that the choice of parameters, $m_u = 0.9$, $m_d = 2.1$, $g = 2$, and $m_{e,\nu} = 0$ results in the desired hierarchy of baryon and lepton masses. The relevant part of the spectrum, obtained from an exact diagonalization of the Hamiltonian, is shown in Table I. Although kinematically allowed, multiple instances of β-decay cannot occur for $L = 1$ as there can be at most one of each (anti)lepton. Note that even though $m_{e,\nu} = 0$, the electron and neutrino are gapped due to the finite spatial volume.

To prepare the Δ^- initial state, we exploit the observation made in Ref. [158] that the stretched-isospin eigenstates of the Δ-baryons, with third component of isospin $I_3 = \pm 3/2$, factorize between the u and d flavor sectors for $L = 1$. Therefore, the previously developed variational quantum eigensolver (VQE) [178] circuit [158] used to prepare the one-flavor vacuum can be used to initialize the two-flavor Δ^- wave function. This is done by initializing the vacuum in the lepton sector, preparing the state $|d_r d_g d_b\rangle$ in the d sector, and applying the VQE circuit to produce the u-sector vacuum. In the tilde basis, the lepton vacuum is the unoccupied state (trivial vacuum), and the complete state-preparation circuit is shown in Fig. 3, where θ is shorthand for RY(θ). The rotation angles are related by

$$\begin{aligned}\theta_0 &= -2\,\sin^{-1}[\tan(\theta/2)\cos(\theta_1/2)],\\ \theta_{00} &= -2\,\sin^{-1}[\tan(\theta_0/2)\cos(\theta_{01}/2)],\\ \theta_{01} &= -2\sin^{-1}[\cos(\theta_{11}/2)\tan(\theta_1/2)]\end{aligned} \tag{13}$$

and, for $m_u = 0.9$ and $g = 2$,[2]

$$\theta = 0.2256, \qquad \theta_1 = 0.4794, \qquad \theta_{11} = 0.3265. \tag{14}$$

In total, state preparation requires the application of nine CNOT gates.

Once the Δ^- baryon state has been initialized on the register of qubits, it is then evolved in time with the full Hamiltonian. The quantum circuits that implement the Trotterized time-evolution induced by H_{quarks} and H_{glue} were previously developed in Ref. [158], where it was found that, by using an ancilla, each Trotter step can be implemented using 114 CNOTs. The lepton Hamiltonian, $\tilde{H}_{\text{leptons}}$, has just single Zs, which are Trotterized with single qubit rotations. The circuits required to implement a Trotter step from $\tilde{H}_\beta$ are similar to those developed in Ref. [158], and their construction is outlined in Appendix E. For the present choice of parameters, the main contribution to the initial (Δ^-) wave function is $|d_b d_g d_r\rangle$, i.e., the quark configuration associated with the

TABLE I. The energy gap above the vacuum of states relevant for β-decays of single baryons with $m_u = 0.9$, $m_d = 2.1$, $g = 2$, and $m_{e,\nu} = 0$. The leptons are degenerate in energy and collectively denoted by l.

Energy of states relevant for β-decay (above the vacuum)	
State	Energy gap
Δ^{++}	2.868
$\Delta^{++} + 2l$	3.868
Δ^{+}	4.048
$\Delta^{++} + 4l$	4.868
$\Delta^{+} + 2l$	5.048
Δ^{0}	5.229
$\Delta^{+} + 4l$	6.048
$\Delta^{0} + 2l$	6.229
Δ^{-}	6.409

[2]The $\bar{u}$ and u parts of the lattice are separated by a fully packed d sector, which implies that the part of the wave functions with odd numbers of anti-up quarks have relative minus signs compared to the one-flavor vacuum wave function.

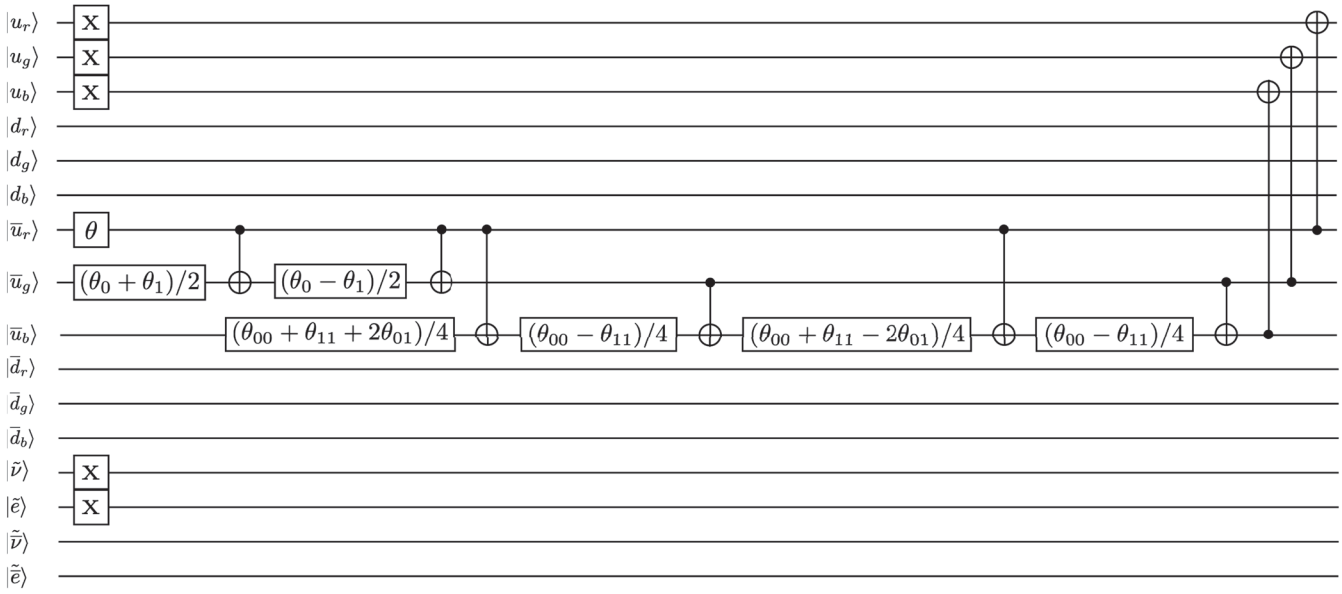

FIG. 3. A quantum circuit that can be used to prepare the Δ^--baryon on $L = 1$ spatial site.

"bare" baryon in the d sector and the trivial vacuum in the u sector. This implies that the dominant contribution to the β-decay is from the $\phi_0^{(u)\dagger}\phi_0^{(d)}\tilde{\chi}_0^{(e)\dagger}\tilde{\chi}_1^{(\nu)}$ term[3] in Eq. (8), which acts only on valence quarks, and the β-decay operator can be approximated by

$$\tilde{H}_\beta^{\rm val} = \frac{G}{\sqrt{2}}\left(\sigma_{\bar{\nu}}^- \sigma_e^+ \sum_{c=r,g,b} \sigma_{d,c}^- Z^2 \sigma_{u,c}^+ + \text{H.c.}\right), \quad (15)$$

for these parameter values. See Appendix H for details on the validity of this approximation. All of the results presented in this section implement this interaction, the Trotterization of which requires 50 CNOTs. Notice that, if the Trotterization of $\tilde{H}_\beta^{\rm val}$ is placed at the end of the first Trotter step, then $U(t) = \exp(-i\tilde{H}_\beta^{\rm val} t) \times \exp\left[-i(\tilde{H}_{\rm leptons} + H_{\rm quarks} + H_{\rm glue})t\right]$, and the initial exponential (corresponding to strong-interaction evolution) can be omitted as it acts on an eigenstate (the Δ^-). This reduces the CNOTs required for one and two Trotter steps to 50 and 214, respectively. For an estimate of the number of CNOTs required to time evolve with the β-decay Hamiltonian on larger lattices, see Appendix F. The probability of β-decay, as computed both through exact diagonalization of the Hamiltonian and through Trotterized time evolution using the `qiskit` classical simulator [179], is shown in Fig. 4. The periodic structure is a finite volume effect, and the probability of β-decay is expected to tend to an exponential in time as L increases; see Appendix D.

[3]Note that the $\phi_0^{(u)\dagger}\phi_0^{(d)}\tilde{\chi}_1^{(e)\dagger}\tilde{\chi}_0^{(\nu)}$ term is suppressed since the lepton vacuum in the tilde basis satisfies $\tilde{\chi}_1^{(e,\nu)\dagger}|\Omega\rangle_{\rm lep} = \tilde{\chi}_0^{(e,\nu)}|\Omega\rangle_{\rm lep} = 0$.

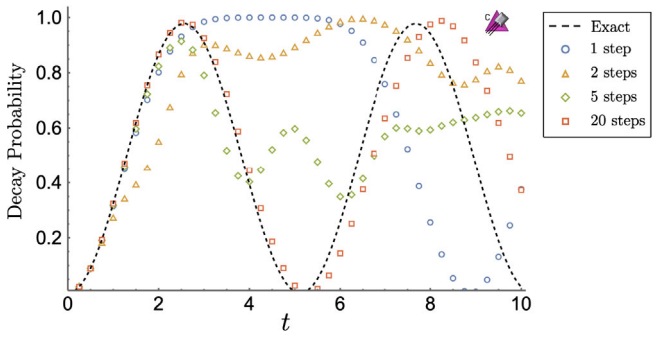

FIG. 4. The probability of β-decay, $\Delta^- \to \Delta^0 + e + \bar{\nu}$, with $m_u = 0.9$, $m_d = 2.1$, $m_{e,\nu} = 0$, $g = 2$, and $G = 0.5$ computed via exact diagonalization (dotted black line) and on the `qiskit` quantum simulator [179] using 1,2,5,20 Trotter steps.

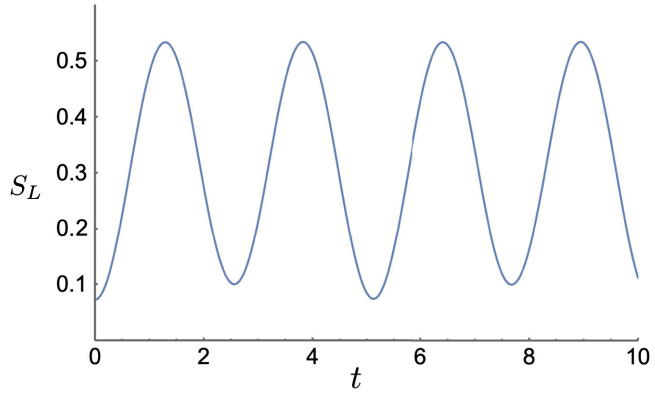

FIG. 5. The linear entanglement entropy, S_L, between quarks and antiquarks plus leptons during the β-decay of an initial Δ^--baryon.

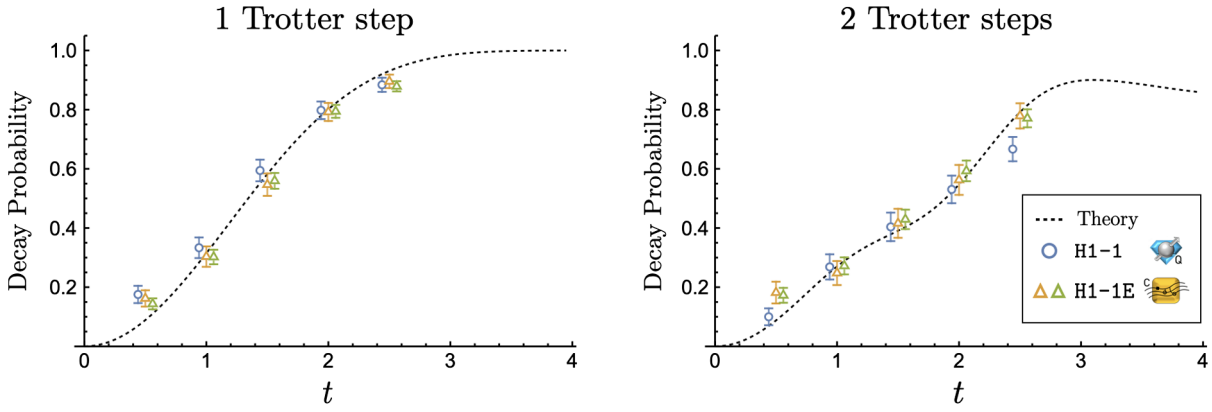

FIG. 6. The probability of β-decay, $\Delta^- \to \Delta^0 + e + \bar{\nu}$, with $m_u = 0.9$, $m_d = 2.1$, $m_{e,\nu} = 0$, $g = 2$, and $G = 0.5$, using one (left panel) and two (right panel) Trotter steps (requiring 59 and 212 ZZ gates, respectively), as given in Table II. The dashed-black curves show the expected result from Trotterized time evolution, corresponding to the blue circles (orange triangles) in Fig. 4 for one (two) Trotter steps. The blue circles correspond to the data obtained on the `H1-1` machine, and the orange (green) triangles to the `H1-1E` emulator, each obtained from 200 shots (400 shots). The points have been shifted slightly along the t axis for clarity. Error mitigation beyond physical-state postselection has not been performed. The weak Hamiltonian in the time evolution responsible for the decay is given in Eq. (15).

Entanglement in quantum simulations of lattice gauge theories is a growing area of focus; see, e.g., Refs. [180–183], and it is interesting to examine the evolution of entanglement during the β-decay process. Before the decay, the quarks and antiquarks are together in a pure state as the leptons are in the vacuum, and subsequent time evolution of the state introduces components into the wave function that have nonzero population of the lepton states. One measure of entanglement is the linear entropy,

$$S_L = 1 - \mathrm{Tr}[\rho_q^2], \tag{16}$$

between the quarks and antiquarks plus leptons. It is constructed by tracing the full density matrix, ρ, over the antiquark and lepton sector to form the reduced density matrix $\rho_q = \mathrm{Tr}_{\bar{q},\mathrm{leptons}}[\rho]$. Figure 5 shows the linear entropy computed through exact diagonalization of the Hamiltonian with the parameters discussed previously in the text. By comparing with the persistence probability in Fig. 4, it is seen that the entanglement entropy evolves at twice the frequency of the β-decay probability. This is because β-decay primarily transitions the baryon between the ground state of the Δ^- and Δ^0. It is expected that these states will have a comparable amount of entanglement, and so the entanglement is approximately the same when the decay probabilities are 0 and 1. While this makes this particular example somewhat uninteresting, it does demonstrate that when multiple final states are accessible, the time dependence of the entanglement structure might be revealing.

B. Simulations using Quantinuum's `H1-1` 20 qubit trapped ion quantum computer

Both the initial state preparation and one and two steps of Trotterized time evolution were executed using Quantinuum's `H1-1` 20 qubit trapped ion quantum computer [176] and its simulator `H1-1E`[4] (for details on the specifications of `H1-1`, see Appendix G). After transpilation onto the native gate set of `H1-1`, a single Trotter step requires 59 ZZ gates, while two Trotter steps requires 212 ZZ gates.[5] By postselecting results on "physical" states with baryon number $B = 1$ and lepton number $L = 0$ to mitigate single-qubit errors (e.g., Ref. [80]), approximately 90% (50%) of the total events from the one (two) Trotter step circuit remained. Additionally, for the two Trotter step circuit, results were selected where the ancilla qubit was in the $|0\rangle$ state (around 95%).[6]

The results of the simulations are shown in Fig. 6 and given in Table II. By comparing the results from `H1-1` and `H1-1E` (using 200 shots) it is seen that the simulator is able to faithfully reproduce the behavior of the quantum computer. The emulator was also run with 400 shots and clearly shows convergence to the expected value, verifying that the agreement between data and theory was not an artifact due to low statistics (and large error bars). Compared with the results presented in Ref. [158] that were performed using IBM's `ibmq_jakarta` and `ibm_perth`, error mitigation techniques were not applied to the present simulations due to the overhead in resource requirements. Specifically, Pauli twirling, dynamical decoupling, decoherence renormalization, and measurement error mitigation were not performed. This is practical

[4]The classical simulator `H1-1E` includes depolarizing gate noise, leakage errors, cross talk noise, and dephasing noise due to transport and qubit idling [177].

[5]The number of ZZ gates could be further reduced by five by not resetting the ancilla.

[6]For this type of error, the midcircuit measurement and reinitialization option available for `H1-1` could have been used to identify the case where the bit flip occurred after the ancilla was used, and the error had no effect on the final results.

TABLE II. The probability of β-decay, $\Delta^- \to \Delta^0 + e + \bar{\nu}$, on $L = 1$ spatial lattice with $m_u = 0.9$, $m_d = 2.1$, $m_{e,\nu} = 0$, $g = 2$, and $G = 0.5$. These simulations were performed using Quantinuum's `H1-1` and `H1-1E` and included the initial state preparation and subsequent time evolution under one and two Trotter steps. The results are displayed in Fig. 6. The columns labeled (×2 stats) were obtained using 400 shots, compared to the rest, that used 200 shots, and uncertainties were computed assuming the results follow a binomial distribution.

Single-baryon decay probabilities using Quantinuum's `H1-1` and `H1-1E`								
	One trotter step				Two trotter steps			
t	`H1-1`	`H1-1E`	`H1-1E` (×2 stats)	Theory	`H1-1`	`H1-1E`	`H1-1E` (×2 stats)	Theory
0.5	0.175(29)	0.162(28)	0.144(19)	0.089	0.100(29)	0.182(37)	0.173(25)	0.088
1.0	0.333(35)	0.303(34)	0.302(25)	0.315	0.269(43)	0.248(41)	0.272(29)	0.270
1.5	0.594(37)	0.547(38)	0.559(27)	0.582	0.404(48)	0.416(49)	0.429(33)	0.391
2.0	0.798(30)	0.792(30)	0.794(22)	0.801	0.530(47)	0.563(51)	0.593(35)	0.547
2.5	0.884(24)	0.896(23)	0.879(17)	0.931	0.667(41)	0.779(43)	0.771(30)	0.792

because the two-qubit gate, state preparation, and measurement (SPAM) errors are an order of magnitude smaller on Quantinuum's trapped-ion system compared to those of IBM's superconducting qubit systems (and a similar error rate on the single-qubit gates) [184].

IV. SPECULATION ABOUT QUANTUM SIMULATIONS WITH A HIERARCHY OF LENGTH SCALES

It is interesting to consider how a hierarchy of length scales, as present in the SM, may be helpful in error correction. In the system we have examined, the low energy strong sector is composed of mesons, baryons, and nuclei, with both color singlet and nonsinglet excitations (existing at higher energies). As observed in Ref. [158], OBCs allow for relatively low-energy colored "edge" states to exist near the boundary of the lattice. The energy of a color nonsinglet grows linearly with its distance from the boundary, leading to a force on colored objects. This will cause colored errors in the bulk to migrate to the edge of the lattice where they could be detected and possibly removed. This is one benefit of using axial gauge, where Gauss's law is automatically enforced, and a colored "error" in the bulk generates a color flux tube that extends to the boundary.

Localized two-bit-flip errors can create color-singlet excitations that do not experience a force toward the boundary, but which are vulnerable to weak decay. For sufficiently large lattices, color singlet excitations will decay weakly down to stable states enabled by the near continuum of lepton states. In many ways, this resembles the quantum imaginary-time evolution (QITE) [185–187] algorithm, which is a special case of coupling to open systems, where quantum systems are driven into their ground state by embedding them in a larger system that acts as a heat reservoir. One can speculate that, in the future, quantum simulations of QCD will benefit from also including electroweak interactions as a mechanism to cool the strongly interacting sector from particular classes of errors.

This particular line of investigation is currently at a "schematic" level, and significantly more work is required to quantify its utility. Given the quantum resource requirements, it is likely that the Schwinger model will provide a suitable system to explore such scenarios.

V. SUMMARY AND CONCLUSIONS

Quantum simulations of SM physics is in its infancy and, for practical reasons, has been previously limited to either QCD or QED in one or two spatial dimensions. In this work, we have started the integration of the electroweak sector into quantum simulations of QCD by examining the time evolution of the β-decay of one baryon. In addition to the general framework that allows for simulations of arbitrary numbers of lattice sites in one dimension, we present results for $L = 1$ spatial lattice site, which requires 16 qubits. Explicitly, this work considered quantum simulations of $\Delta^- \to \Delta^0 e\bar{\nu}$ in two flavor $1 + 1$D QCD for $L = 1$ spatial lattice site. Simulations were performed using Quantinuum's `H1-1` 20-qubit trapped ion quantum computer and classical simulator `H1-1E`, requiring 17 (16 system and one ancilla) qubits. Results were presented for both one and two Trotter steps, including the state preparation of the initial baryon, requiring 59 and 212 two-qubit gates, respectively. Even with 212 two-qubit gates, `H1-1` provided results that are consistent with the expected results, within uncertainties, without error-mitigation beyond physical-state postselection. While not representative of β-decay in the continuum, these results demonstrate the potential of quantum simulations to determine the real-time evolution of decay and reaction processes in nuclear and high-energy processes. High temporal-resolution studies of the evolution of the quarks and gluons during hadronic decays and nuclear reactions are expected to provide new insights into the mechanisms responsible for these processes and lead to new strategies for further reducing systematic errors in their prediction.

ACKNOWLEDGMENTS

We would like to thank Silas Beane, Natalie Klco, and Randy Lewis for helpful discussions and comments. This work was supported, in part, by the U.S. Department of Energy grant DE-FG02-97ER-41014 (Farrell), the U.S. Department of Energy, Office of Science, Office of Nuclear Physics, InQubator for Quantum Simulation (IQuS) (https://iqus.uw.edu) under Award Number DOE (NP) Award DE-SC0020970 (Chernyshev, Farrell, Powell, Savage, Zemlevskiy), and the Quantum Science Center (QSC) (https://qscience.org), a National Quantum Information Science Research Center of the U.S. Department of Energy (DOE) (Illa). This work is also supported, in part, through the Department of Physics (https://phys.washington.edu) and the College of Arts and Sciences (https://www.artsci.washington.edu) at the University of Washington. This research used resources of the Oak Ridge Leadership Computing Facility, which is a DOE Office of Science User Facility supported under Contract DE-AC05-00OR22725. We have made extensive use of Wolfram `Mathematica` [188], `python` [189,190], `julia` [191], `jupyter` notebooks [192] in the `Conda` environment [193], and the quantum programming environments: Google's `cirq` [194], IBM's `qiskit` [179], and CQC's `pytket` [195].

APPENDIX A: THE COMPLETE SPIN HAMILTONIAN FOR $L=1$

After the JW mapping of the Hamiltonian to qubits, and using the tilde basis for the leptons, the four contributing terms are

$$H = H_{\text{quarks}} + \tilde{H}_{\text{leptons}} + H_{\text{glue}} + \tilde{H}_{\beta}, \tag{A1a}$$

$$\begin{aligned} H_{\text{quarks}} = {} & \frac{1}{2}[m_u(Z_0+Z_1+Z_2-Z_6-Z_7-Z_8+6)+m_d(Z_3+Z_4+Z_5-Z_9-Z_{10}-Z_{11}+6)] \\ & -\frac{1}{2}(\sigma_6^+Z_5Z_4Z_3Z_2Z_1\sigma_0^- + \sigma_6^-Z_5Z_4Z_3Z_2Z_1\sigma_0^+ + \sigma_7^+Z_6Z_5Z_4Z_3Z_2\sigma_1^- + \sigma_7^-Z_6Z_5Z_4Z_3Z_2\sigma_1^+ \\ & + \sigma_8^+Z_7Z_6Z_5Z_4Z_3\sigma_2^- + \sigma_8^-Z_7Z_6Z_5Z_4Z_3\sigma_2^+ + \sigma_9^+Z_8Z_7Z_6Z_5Z_4\sigma_3^- + \sigma_9^-Z_8Z_7Z_6Z_5Z_4\sigma_3^+ \\ & + \sigma_{10}^+Z_9Z_8Z_7Z_6Z_5\sigma_4^- + \sigma_{10}^-Z_9Z_8Z_7Z_6Z_5\sigma_4^+ + \sigma_{11}^+Z_{10}Z_9Z_8Z_7Z_6\sigma_5^- + \sigma_{11}^-Z_{10}Z_9Z_8Z_7Z_6\sigma_5^+), \end{aligned} \tag{A1b}$$

$$\begin{aligned} \tilde{H}_{\text{leptons}} = {} & \frac{1}{4}\sqrt{1+4m_e^2}(Z_{13}-Z_{15}) + \frac{1}{4}\sqrt{1+4m_\nu^2}(Z_{12}-Z_{14}) \\ H_{\text{glue}} = {} & \frac{g^2}{2}\left[\frac{1}{3}(3-Z_1Z_0-Z_2Z_0-Z_2Z_1) + \sigma_4^+\sigma_3^-\sigma_1^-\sigma_0^+ + \sigma_4^-\sigma_3^+\sigma_1^+\sigma_0^- + \sigma_5^+Z_4\sigma_3^-\sigma_2^-Z_1\sigma_0^+ + \sigma_5^-Z_4\sigma_3^+\sigma_2^+Z_1\sigma_0^- \right. \\ & + \sigma_5^+\sigma_4^-\sigma_2^-\sigma_1^+ + \sigma_5^-\sigma_4^+\sigma_2^+\sigma_1^- \\ & \left. + \frac{1}{12}(2Z_3Z_0+2Z_4Z_1+2Z_5Z_2-Z_5Z_0-Z_5Z_1-Z_4Z_2-Z_4Z_0-Z_3Z_1-Z_3Z_2)\right], \end{aligned} \tag{A1c}$$

$$\begin{aligned} \tilde{H}_{\beta} = {} & \frac{G}{\sqrt{2}}\left\{\frac{1}{2}(s_+^es_+^\nu + s_-^es_-^\nu)[(\sigma_{14}^-\sigma_{13}^+ - \sigma_{15}^+Z_{14}Z_{13}\sigma_{12}^-)(\sigma_3^-Z_2Z_1\sigma_0^+ + \sigma_4^-Z_3Z_2\sigma_1^+ + \sigma_5^-Z_4Z_3\sigma_2^+ + \sigma_9^-Z_8Z_7\sigma_6^+ \right. \\ & + \sigma_{10}^-Z_9Z_8\sigma_7^+ + \sigma_{11}^-Z_{10}Z_9\sigma_8^+) + (\sigma_{14}^+\sigma_{13}^- - \sigma_{15}^-Z_{14}Z_{13}\sigma_{12}^+)(\sigma_3^+Z_2Z_1\sigma_0^- + \sigma_4^+Z_3Z_2\sigma_1^- + \sigma_5^+Z_4Z_3\sigma_2^- \\ & \left. + \sigma_9^+Z_8Z_7\sigma_6^- + \sigma_{10}^+Z_9Z_8\sigma_7^- + \sigma_{11}^+Z_{10}Z_9\sigma_8^-)] \right. \\ & -\frac{1}{2}(s_+^es_-^\nu + s_-^es_+^\nu)[(\sigma_{14}^-\sigma_{13}^+ + \sigma_{15}^+Z_{14}Z_{13}\sigma_{12}^-)(\sigma_9^-Z_8Z_7Z_6Z_5Z_4Z_3Z_2Z_1\sigma_0^+ + \sigma_{10}^-Z_9Z_8Z_7Z_6Z_5Z_4Z_3Z_2\sigma_1^+ \\ & + \sigma_{11}^-Z_{10}Z_9Z_8Z_7Z_6Z_5Z_4Z_3\sigma_2^+ + \sigma_6^+Z_5Z_4\sigma_3^- + \sigma_7^+Z_6Z_5\sigma_4^- + \sigma_8^+Z_7Z_6\sigma_5^-) \\ & + (\sigma_{14}^+\sigma_{13}^- + \sigma_{15}^-Z_{14}Z_{13}\sigma_{12}^+)(\sigma_9^+Z_8Z_7Z_6Z_5Z_4Z_3Z_2Z_1\sigma_0^- + \sigma_{10}^+Z_9Z_8Z_7Z_6Z_5Z_4Z_3Z_2\sigma_1^- \\ & \left. + \sigma_{11}^+Z_{10}Z_9Z_8Z_7Z_6Z_5Z_4Z_3\sigma_2^- + \sigma_6^-Z_5Z_4\sigma_3^+ + \sigma_7^-Z_6Z_5\sigma_4^+ + \sigma_8^-Z_7Z_6\sigma_5^+)]\right\}. \end{aligned} \tag{A1d}$$

In the mapping, the qubits are indexed right to left and, for example, qubit zero (one) corresponds to a red (green) up quark.

APPENDIX B: β-DECAY IN THE STANDARD MODEL

To put our simulations in $1+1$D into context, it is helpful to outline relevant aspects of single-hadron β-decays in the SM in $3+1$D. Far below the electroweak symmetry-breaking scale, charged-current interactions can be included as an infinite set of effective operators in a systematic EFT description, ordered by their contributions in powers of low-energy scales divided by appropriate powers of M_W. For instance, β-decay rates between hadrons scale as $\sim\Lambda(G_F\Lambda^2)^2(\Lambda/M_W)^n$, where Λ denotes the low-energy scales, $\frac{G_F}{\sqrt{2}}=\frac{g_2^2}{8M_W^2}$ is Fermi's constant, and LO (in Λ/M_W) corresponds to $n=0$. By matching operators at LO in SM interactions, the β-decay of the neutron is induced by an effective Hamiltonian density of the form [13,171]

$$\mathcal{H}_\beta=\frac{G_F}{\sqrt{2}}V_{ud}\bar{\psi}_u\gamma^\mu(1-\gamma_5)\psi_d\bar{\psi}_e\gamma_\mu(1-\gamma_5)\psi_{\nu_e}+\text{H.c.}, \tag{B1}$$

where V_{ud} is the element of the CKM matrix for $d\to u$ transitions. As $\mathcal{H}_\beta$ factors into contributions from lepton and quark operators, the matrix element factorizes into a plane-wave lepton contribution and a nonperturbative hadronic component requiring matrix elements of the quark operator between hadronic states. With the mass hierarchies and symmetries in nature, there are two dominant form factors, so that

$$\begin{aligned}&\langle p(p_p)|\bar{\psi}_u\gamma^\mu(1-\gamma_5)\psi_d|n(p_n)\rangle\\&\quad=\bar{U}_p[g_V(q^2)\gamma^\mu-g_A(q^2)\gamma^\mu\gamma_5]U_n,\end{aligned} \tag{B2}$$

where q is the four-momentum transfer of the process, $g_V(0)=1$ in the isospin limit, and $g_A(0)=1.2754(13)$ [196] as measured in experiment. The matrix element for $n\to pe^-\bar{\nu}_e$ calculated from the Hamiltonian in Eq. (B1) is

$$\begin{aligned}|\mathcal{M}|^2&=16G_F^2|V_{ud}|^2M_nM_p(g_V^2+3g_A^2)\\&\quad\times\left(E_\nu E_e+\frac{g_V^2-g_A^2}{g_V^2+3g_A^2}\mathbf{p}_e\cdot\mathbf{p}_{\bar{\nu}}\right),\end{aligned} \tag{B3}$$

which leads to a neutron width of (at LO in $(M_n-M_p)/M_n$ and m_e/M_n)

$$\Gamma_n=\frac{G_F^2|V_{ud}|^2(M_n-M_p)^5}{60\pi^3}(g_V^2+3g_A^2)f'(y), \tag{B4}$$

where $f'(y)$ is a phase-space factor,

$$\begin{aligned}f'(y)&=\sqrt{1-y^2}\left(1-\frac{9}{2}y^2-4y^4\right)\\&\quad-\frac{15}{2}y^4\log\left[\frac{y}{\sqrt{1-y^2}+1}\right],\end{aligned} \tag{B5}$$

and $y=m_e/(M_n-M_p)$. Radiative effects, recoil effects, and other higher-order contributions have been neglected.

APPENDIX C: β-DECAY IN 1+1 DIMENSIONS: THE $L=\infty$ AND CONTINUUM LIMITS

In $1+1$D, the fermion field has dimensions $[\psi]=\frac{1}{2}$, and a four-Fermi operator has dimension $[\hat{\theta}]=2$. Therefore, while in $3+1$D $[G_F]=-2$, in $1+1$D, the coupling has dimension $[G]=0$. For our purposes, to describe the $\beta-$Decay of a Δ^--baryon in $1+1$D, we have chosen to work with an effective Hamiltonian of the form

$$\begin{aligned}\mathcal{H}_\beta^{1+1}&=\frac{G}{\sqrt{2}}\bar{\psi}_u\gamma^\mu\psi_d\bar{\psi}_e\gamma_\mu\psi_{\bar{\nu}}+\text{H.c.}\\&=\frac{G}{\sqrt{2}}\bar{\psi}_u\gamma^\mu\psi_d\bar{\psi}_e\gamma_\mu\mathcal{C}\psi_\nu+\text{H.c.},\end{aligned} \tag{C1}$$

where we have chosen the basis

$$\begin{aligned}&\gamma_0=\begin{pmatrix}1&0\\0&-1\end{pmatrix},\quad\gamma_1=\begin{pmatrix}0&1\\-1&0\end{pmatrix}=\mathcal{C},\quad\gamma_0\gamma_\mu^\dagger\gamma_0=\gamma_\mu,\\&\gamma_0\mathcal{C}^\dagger\gamma_0=\mathcal{C},\quad\{\gamma_\mu,\gamma_\nu\}=2g_{\mu\nu}.\end{aligned} \tag{C2}$$

For simplicity, the CKM matrix element is set equal to unity as only one generation of particles is considered.

In the limit of exact isospin symmetry, which we assume to be approximately valid in this appendix, the four Δ baryons form an isospin quartet and can be embedded in a tensor T^{abc} (as is the case for the Δ resonances in nature) as $T^{111}=\Delta^{++}$, $T^{112}=T^{121}=T^{211}=\Delta^+/\sqrt{3}$, $T^{122}=T^{221}=T^{212}=\Delta^0/\sqrt{3}$, $T^{222}=\Delta^-$. Matrix elements of the isospin generators are reproduced by an effective operator of the form

$$\bar{\psi}_q\gamma^\mu\tau^\alpha\psi_q\to3\bar{T}_{abc}\gamma^\mu(\tau^\alpha)_d^cT^{abd}, \tag{C3}$$

which provides a Clebsch-Gordan coefficient for isospin raising operators,

$$\begin{aligned}\bar{\psi}_q\gamma^\mu\tau^+\psi_q\to&\sqrt{3}\,\overline{\Delta^{++}}\gamma^\mu\Delta^+ + 2\overline{\Delta^+}\gamma^\mu\Delta^0\\&+\sqrt{3}\,\overline{\Delta^0}\gamma^\mu\Delta^-.\end{aligned} \tag{C4}$$

The matrix element for β-decay factorizes at LO in the electroweak interactions. The hadronic component of the matrix element is given by

$$\begin{aligned}\langle \Delta^0(p_0)|\bar{\psi}_u\gamma^\alpha\psi_d|\Delta^-(p_-)\rangle &= \sqrt{3}g_V(q^2)\bar{U}_{\Delta^0}\gamma^\alpha U_{\Delta^-} = H^\alpha,\\ H^\alpha H^{\beta\dagger} &= 3|g_V(q^2)|^2\mathrm{Tr}[\gamma^\alpha(\not{p}_- + M_{\Delta^-})\gamma^\beta(\not{p}_0 + M_{\Delta^0})]\\ &= 6|g_V(q^2)|^2[p_-^\alpha p_0^\beta + p_0^\alpha p_-^\beta - g^{\alpha\beta}(p_-\cdot p_0) + M_{\Delta^-}M_{\Delta^0}g^{\alpha\beta}] = H^{\alpha\beta},\end{aligned} \tag{C5}$$

and the leptonic component of the matrix element is given by, assuming that the electron and neutrino are massless,

$$\begin{aligned}\langle e^-\bar{\nu}_e|\bar{\psi}_e\gamma^\alpha C\psi_\nu|0\rangle &= \bar{U}_e\gamma^\alpha C V_\nu = L^\alpha,\\ L^\alpha L^{\beta\dagger} &= \mathrm{Tr}[\gamma^\alpha C\not{p}_\nu C\gamma^\beta \not{p}_e] = \mathrm{Tr}[\gamma^\alpha\not{p}_\nu\gamma^\beta\not{p}_e] = 2[\bar{p}_\nu^\alpha p_e^\beta + \bar{p}_\nu^\beta p_e^\alpha - g^{\alpha\beta}(\bar{p}_\nu\cdot p_e)] = L^{\alpha\beta},\end{aligned} \tag{C6}$$

where $p = (p^0, +p^1)$ and $\bar{p} = (p^0, -p^1)$. Therefore, the squared matrix element of the process is

$$|\mathcal{M}|^2 = \frac{G^2}{2}H^{\alpha\beta}L_{\alpha\beta} = 12G^2g_V^2M_{\Delta^-}(M_{\Delta^-} - 2E_{\bar{\nu}})(E_eE_{\bar{\nu}} - \mathbf{p}_e\cdot\mathbf{p}_{\bar{\nu}}), \tag{C7}$$

from which the delta decay width can be determined by standard methods,

$$\begin{aligned}\Gamma_{\Delta^-} &= \frac{1}{2M_{\Delta^-}}\int\frac{d\mathbf{p}_e}{4\pi E_e}\frac{d\mathbf{p}_{\bar{\nu}}}{4\pi E_{\bar{\nu}}}\frac{d\mathbf{p}_0}{4\pi E_0}(2\pi)^2\delta^2(p_- - p_0 - p_e - p_{\bar{\nu}})|\mathcal{M}|^2\\ &= 3\frac{G^2g_V^2}{2\pi}\int dE_e dE_{\bar{\nu}}\delta(Q - E_e - E_{\bar{\nu}}) + \mathcal{O}(Q^n/M_\Delta^n)\\ &= 3\frac{G^2g_V^2Q}{2\pi} + \mathcal{O}(Q^n/M_\Delta^n),\end{aligned} \tag{C8}$$

where $Q = M_{\Delta^-} - M_{\Delta^0}$, and we have retained only the leading terms in an expansion in Q/M_Δ and evaluated the vector form factor at $g_V(q^2 = 0) \equiv g_V$. The electron and neutrino masses have been set to zero, and the inclusion of nonzero masses will lead to a phase-space factor, f_1, reducing the width shown in Eq. (C8), and which becomes $f_1 = 1$ in the massless limit.

APPENDIX D: β-DECAY IN 1 + 1 DIMENSIONS: FINITE L AND NONZERO SPATIAL LATTICE SPACING

The previous appendix computed the β-decay rate in $1 + 1$D in infinite volume and in the continuum. However, lattice calculations of such processes will necessarily be performed with a nonzero lattice spacing and a finite number of lattice points. For calculations done on a Euclidean-space lattice, significant work has been done to develop the machinery used to extract physically meaningful results. This formalism was initially pioneered by Lüscher [197–199] for hadron masses and two-particle scattering and has been extended to more complex systems relevant to electroweak processes (Lellouch-Lüscher) [200–215] and to nuclear physics [201,208,216–227]. Lüscher's method was originally derived from an analysis of Hamiltonian dynamics in Euclidean space and later from a field theoretic point of view directly from correlation functions. The challenge is working around the Maiani-Testa theorem [228] and reliably determining Minkowski-space matrix elements from Euclidean-space observables. This formalism has been used successfully for a number of important quantities and continues to be the workhorse for Euclidean-space computations.

As quantum simulations provide observables directly in Minkowski space, understanding the finite-volume and nonzero lattice spacing artifacts requires a similar but different analysis than in Euclidean space.[7] While the method used in Euclidean space of determining S-matrix elements for scattering processes from energy eigenvalues can still be applied, Minkowski space simulations will also allow for a direct evaluation of scattering processes, removing some of the modeling that remains in Euclidean-space calculations.[8] Neglecting electroweak interactions beyond β-decay means that the final state leptons are non interacting (plane waves when using periodic boundary conditions), and therefore the modifications to the density of states due to interactions, as encapsulated within the Lüscher formalism, are absent.

With Hamiltonian evolution of a system described within a finite-dimensional Hilbert space, the persistence amplitude of the initial state coupled to final states via the

[7]Estimates of such effects in model $1 + 1$ dimensional simulations can be found in Ref. [229].

[8]For example, the energies of states in different volumes are different, and so the elements of the scattering matrix are constrained over a range of energies and not at one single energy, and *a priori* unknown interpolations are modeled.

weak Hamiltonian will be determined by the sum over oscillatory amplitudes. For a small number of final states, the amplitude will return to unity after some finite period of time. As the density of final states near the energy of the initial state becomes large, there will be cancellations among the oscillatory amplitudes, and the persistence probability will begin to approximate the "classic" exponential decay over some time interval. This time interval will extend to infinity as the density of states tends to a continuous spectrum. It is important to understand how to reliably extract an estimate of the decay rate, with a quantification of systematic errors, from the amplitudes measured in a quantum simulation. This is the subject of future work, but here, a simple model will be used to demonstrate some of the relevant issues.

Consider the weak decay of a strong eigenstate in one sector to a strong eigenstate in a different sector (a sector is defined by its strong quantum numbers). For this demonstration, we calculate the persistence probability of the initial state, averaged over random weak and strong Hamiltonians and initial states, as the number of states below a given energy increases (i.e., increasing density of states). Concretely, the energy eigenvalues of the initial strong sector range from 0 to 1.1, and 10 are selected randomly within this interval. The initial state is chosen to be the one with the fifth lowest energy. The eigenvalues in the final strong sector range between 0 and 2.03, and $Y_f =$ 20 to 400 are selected. The weak Hamiltonian that induces transitions between the 10 initial states to the Y_f final states is a dense matrix with each element selected randomly. The weak coupling constant is scaled so that $G^2\rho_f$ is independent of the number of states, where ρ_f is the density of states. This allows for a well-defined persistence probability as $Y_f \to \infty$. For this example, the elements of the weak Hamiltonian were chosen between $\pm w_f$, where $w_f = 1/(2\sqrt{Y_F})$. Figure 7 shows the emergence of the expected exponential decay as the number of available final states tends toward a continuous spectrum. In a quantum simulation of a lattice theory, the density of states increases with L, and the late-time deviation from exponential decay will exhibit oscillatory behavior, as opposed to the plateaus found in this statistically averaged model. The very early time behavior of the probability is interesting to note and exhibits a well-known behavior, e.g., Refs. [230,231]. It is, as expected, not falling exponentially, which sets in over timescales set by the energy spectrum of final states.

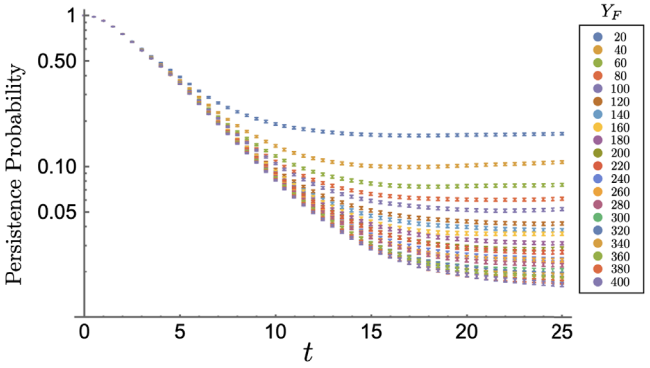

FIG. 7. Ensemble averages (over 2000 random samples) of the persistence probability of an initial state in one sector of a strong Hamiltonian undergoing weak decay to states in a different sector, as described in this appendix. The different colored points are results from calculations with an increasing number of final states, Y_F. The weak coupling scales so that the decay probability converges to a well-defined value as the density of final states tends to a continuum.

Only small lattices are practical for near-term simulation, and lattice artifacts will be important to quantify. Relative to the continuum, a finite lattice spacing modifies the energy-momentum relation and introduces a momentum cutoff on the spectra. However, if the initial particle has a mass that is much less than the cutoff, these effects should be minimal as the energy of each final state particle is bounded above by the mass of the initial particle. As has been shown in this appendix, working on a small lattice with its associated sparse number of final states will lead to significant systematic errors when extracting the decay rates directly from the persistence probabilities. Further work will be necessary to determine how to reliably estimate these errors.

APPENDIX E: β-DECAY CIRCUITS

The quantum circuits that implement the Trotterized time evolution of the β-decay Hamiltonian are similar to those presented in Ref. [158] to implement the strong-interaction dynamics, and here, the differences between the two will be highlighted. The β-decay Hamiltonian in both the standard and tilde layouts, Eqs. (5) and (10), contains terms of the form

$$\begin{aligned} H_\beta &\sim (\sigma^-\sigma^+\sigma^-\sigma^+ + \text{H.c.}) + (\sigma^-\sigma^+\sigma^+\sigma^- + \text{H.c.}) \\ &= \frac{1}{8}(XXXX + YYXX - YXYX + YXXY + XYYX - XYXY + XXYY + YYYY) \\ &\quad + \frac{1}{8}(XXXX + YYXX + YXYX - YXXY - XYYX + XYXY + XXYY + YYYY), \end{aligned} \tag{E1}$$

which can be diagonalized by the GHZ state-preparation circuits, G and $\hat{G}$, shown in Fig. 8. In the GHZ basis, it is found that

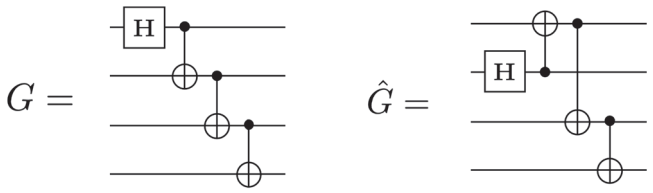

FIG. 8. Two GHZ state preparation circuits.

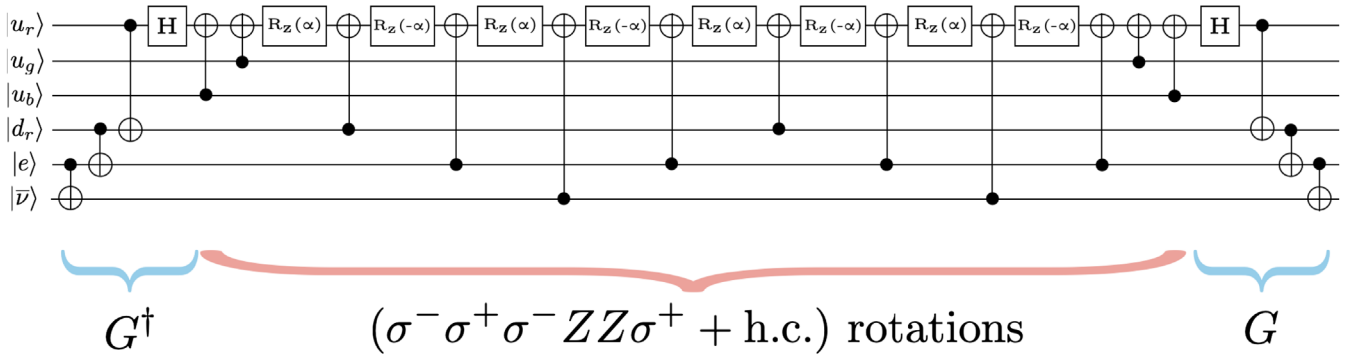

FIG. 9. A quantum circuit that provides the time evolution associated with the $\sigma^-_{\bar{\nu}}\sigma^+_e\sigma^-_{d,r}Z_{u,b}Z_{u,g}\sigma^+_{u,r}$ operator in the β-decay Hamiltonian, with $\alpha = \sqrt{2}Gt/8$.

$$G^\dagger(XXXX + YYXX - YXYX + YXXY + XYYX - XYXY + XXYY + YYYY)G$$
$$= IIIZ - ZIIZ + ZZIZ - ZZZZ - IZIZ + IZZZ - IIZZ + ZIZZ, \tag{E2}$$

and

$$\hat{G}^\dagger(XXXX + YYXX + YXYX - YXXY - XYYX + XYXY + XXYY + YYYY)\hat{G}$$
$$= IIZI - ZIZI - ZZZZ + ZZZI + IZZZ - IZZI - IIZZ + ZIZZ. \tag{E3}$$

Once diagonalized, the circuit is a product of diagonal rotations; see Fig. 9 for an example of the quantum circuit that provides the time evolution associated with $\sigma^-_{\bar{\nu}}\sigma^+_e\sigma^-_{d,r}Z_{u,b}Z_{u,g}\sigma^+_{u,r}$. By diagonalizing with both G and $\hat{G}$ and arranging terms in the Trotterization so that operators that act on the same quarks are next to each other, many of the CNOTs can be made to cancel. Also, an ancilla can be used to efficiently store the parity of the string of Zs between the $\sigma^\pm$.

APPENDIX F: RESOURCE ESTIMATES FOR SIMULATING β-DECAY DYNAMICS

For multiple lattice sites, it is inefficient to work with leptons in the tilde basis. This is due to the mismatch between the local four-Fermi interaction and the non-local tilde basis eigenstates. As a result, the number of terms in the β-decay component of the Hamiltonian will

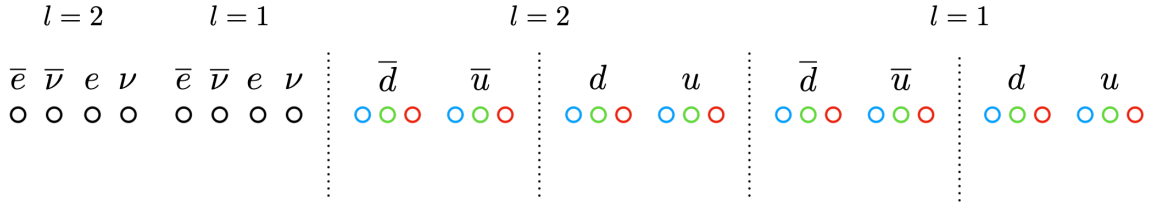

FIG. 10. A qubit layout that is efficient for the simulation of β-decay. Shown is an example for $L = 2$.

scale as $\mathcal{O}(L^2)$ in the tilde basis, as opposed to $\mathcal{O}(L)$ in the local occupation basis. This appendix explores a layout different from the one in Fig. 1, which is optimized for the simulation of β-decay on larger lattices. To minimize the length of JW Z strings, all leptons are placed at the end of the lattice; see Fig. 10. After applying the JW mapping, the β-decay operator becomes

$$\begin{aligned} H_\beta \to \frac{G}{\sqrt{2}} \sum_{l=0}^{L-1} \sum_{c=0}^{2} (&\sigma^-_{l,\bar{\nu}} \sigma^+_{l,e} \sigma^-_{l,d,c} Z^2 \sigma^+_{l,u,c} - \sigma^+_{l,\bar{e}} Z^2 \sigma^-_{l,\nu} \sigma^-_{l,d,c} Z^2 \sigma^+_{l,u,c} + \sigma^-_{l,\bar{\nu}} \sigma^+_{l,e} \sigma^-_{l,\bar{d},c} Z^2 \sigma^+_{l,\bar{u},c} \\ &- \sigma^+_{l,\bar{e}} Z^2 \sigma^-_{l,\nu} \sigma^-_{l,\bar{d},c} Z^2 \sigma^+_{l,\bar{u},c} + \sigma^+_{l,e} \sigma^-_{l,\nu} \sigma^-_{l,\bar{d},c} Z^8 \sigma^+_{l,u,c} - \sigma^+_{l,\bar{e}} \sigma^-_{l,\bar{\nu}} \sigma^-_{l,\bar{d},c} Z^8 \sigma^+_{l,u,c} \\ &+ \sigma^+_{l,e} \sigma^-_{l,\nu} \sigma^+_{l,\bar{u},c} Z^2 \sigma^-_{l,d,c} - \sigma^+_{l,\bar{e}} \sigma^-_{l,\bar{\nu}} \sigma^+_{l,\bar{u},c} Z^2 \sigma^-_{l,d,c} + \text{H.c.}). \end{aligned} \tag{F1}$$

Using the techniques outlined in Appendix E to construct the relevant quantum circuits, the resources required per Trotter step of H_β are estimated to be

$$\begin{aligned} R_Z &: 192L, \\ \text{Hadamard} &: 48L, \\ \text{CNOT} &: 436L. \end{aligned} \tag{F2}$$

For small lattices, $L \lesssim 5$, it is expected that use of the tilde basis will be more efficient, and these estimates should be taken as an upper bound. Combining this with the resources required to time evolve with the rest of the Hamiltonian, see Ref. [158], the total resource requirements per Trotter step are estimated to be

$$\begin{aligned} R_Z &: 264L^2 - 54L + 77, \\ \text{Hadamard} &: 48L^2 + 20L + 2, \\ \text{CNOT} &: 368L^2 + 120L + 74. \end{aligned} \tag{F3}$$

It is important to note that the addition of H_β does not contribute to the quadratic scaling of resources as it is a local operator. Recently, the capability to produce multiqubit gates natively with similar fidelities to two-qubit gates has also been demonstrated [232–234]. This could lead to dramatic reductions in the resources required and, for example, the number of multiqubit terms in the Hamiltonian scales as

$$\text{Multiqubit terms} : 96L^2 - 68L + 22. \tag{F4}$$

TABLE III. The CNOT-gate requirements to perform one Trotter step of time evolution of β-decay for a selection of lattice sizes. For comparison, the number of multiqubit terms in the Hamiltonian is also given.

L	CNOTS	Multiqubit terms
5	9874	2082
10	38,074	8942
50	926,074	236,622
100	3,692,074	953,222

The required number of CNOTs and, for comparison, the number of multiqubit terms in the Hamiltonian, for a selection of different lattice sizes are given in Table III. Note that these estimates do not include the resources required to prepare the initial state.

APPENDIX G: TECHNICAL DETAILS ON THE QUANTINUUM H1-1 QUANTUM PROCESSOR

For completeness, this appendix contains a brief description of Quantinuum's H1-1 20 trapped ion quantum computer (more details can be found in [235]). The H1-1 system uses the System Model H1 design, where unitary operations act on a single line of $^{172}Y^+$ ions induced by lasers. The qubits are defined as the two hyperfine clock states in the $^2S_{1/2}$ ground state of $^{172}Y^+$. Since the physical position of the ions can be modified, it is possible to apply two-qubit gates to any pair of qubits, endowing the device with all-to-all connectivity. Moreover, there are five different physical regions where these gates can be applied in parallel. Although we did not use this feature, it is also possible to perform a midcircuit measurement of a qubit, i.e., initialize it and reuse it (if necessary).

The native gate set for H1-1 is the following,

$$\begin{aligned} U_{1q}(\theta,\phi) &= e^{-i\frac{\theta}{2}[\cos(\phi)X + \sin(\phi)Y]}, \qquad R_Z(\lambda) = e^{-i\frac{\lambda}{2}Z}, \\ ZZ &= e^{-i\frac{\pi}{4}ZZ}, \end{aligned} \tag{G1}$$

where θ in $U_{1q}(\theta,\phi)$ can only take the values $\{\frac{\pi}{2},\pi\}$, and arbitrary values of θ can be obtained by combining several single-qubit gates, $\tilde{U}_{1q}(\theta,\phi) = U_{1q}(\frac{\pi}{2},\phi+\frac{\pi}{2}).R_Z(\theta).U_{1q}(\frac{\pi}{2},\phi-\frac{\pi}{2})$. Translations between

TABLE IV. Errors on the single-qubit, two-qubit, and SPAM operations, with their minimum, average, and maximum values.

	Min	Average	Max
Single-qubit infidelity	2×10^{-5}	5×10^{-5}	3×10^{-4}
Two-qubit infidelity	2×10^{-3}	3×10^{-3}	5×10^{-3}
SPAM error	2×10^{-3}	3×10^{-3}	5×10^{-3}

the gates used in the circuits shown in the main text and appendices to the native ones are performed automatically by `pytket` [195]. The infidelity of the single- and two-qubit gates, as well as the error of the SPAM operations, are shown in Table IV.

APPENDIX H: TIME EVOLUTION UNDER THE FULL β-DECAY OPERATOR

The simulations performed in Sec. III kept only the terms in the β-decay Hamiltonian, which act on valence quarks, see Eq. (15). This appendix examines how well this valence quark β-decay operator approximates the full operator, Eq. (10), for the parameters used in the main text. Shown in Fig. 11 is the decay probability when evolved with both the approximate and full operator as calculated through exact diagonalization of the Hamiltonian. The full β-decay operator has multiple terms that can interfere leading to a more jagged decay probability. The simulations ran on `H1-1` only went out to $t = 2.5$ where the error of the approximate operator is $\sim$20%.

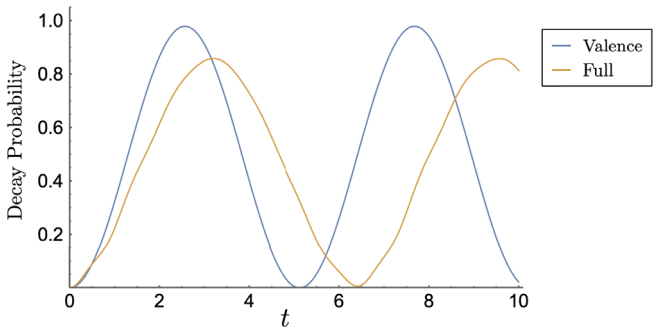

FIG. 11. The probability of β-decay using both the approximate β-decay operator, which only acts on valence quarks (blue) and the full operator (orange).

[1] The Nobel Prize Organization, The Nobel Prize in Chemistry 1999 (1999), https://www.nobelprize.org/prizes/chemistry/1999/zewail/facts/.

[2] Jamie Durrani, Caught on camera the transition state is giving up its secrets (2020), https://www.chemistryworld.com/holy-grails/the-grails/observing-the-transition-state.

[3] S. Glashow, Partial symmetries of weak interactions, Nucl. Phys. **22**, 579 (1961).

[4] P. W. Higgs, Broken Symmetries and the Masses of Gauge Bosons, Phys. Rev. Lett. **13**, 508 (1964).

[5] S. Weinberg, A Model of Leptons, Phys. Rev. Lett. **19**, 1264 (1967).

[6] A. Salam, Weak and electromagnetic interactions, Conf. Proc. C **680519**, 367 (1968).

[7] N. Cabibbo, Unitary Symmetry and Leptonic Decays, Phys. Rev. Lett. **10**, 531 (1963).

[8] M. Kobayashi and T. Maskawa, *CP* violation in the renormalizable theory of weak interaction, Prog. Theor. Phys. **49**, 652 (1973).

[9] M. González-Alonso, O. Naviliat-Cuncic, and N. Severijns, New physics searches in nuclear and neutron beta-decay, Prog. Part. Nucl. Phys. **104**, 165 (2019).

[10] M. T. Hassan *et al.*, Measurement of the neutron decay electron-antineutrino angular correlation by the aCORN experiment, Phys. Rev. C **103**, 045502 (2021).

[11] A. Algora, J. L. Tain, B. Rubio, M. Fallot, and W. Gelletly, Beta-decay studies for applied and basic nuclear physics, Eur. Phys. J. A **57**, 85 (2021).

[12] J. C. Hardy and I. S. Towner, Superallowed $0^+ \to 0^+$ nuclear β decays: 2020 critical survey, with implications for V_{ud} and CKM unitarity, Phys. Rev. C **102**, 045501 (2020).

[13] R. P. Feynman and M. Gell-Mann, Theory of Fermi interaction, Phys. Rev. **109**, 193 (1958).

[14] A. Baroni, L. Girlanda, S. Pastore, R. Schiavilla, and M. Viviani, Nuclear axial currents in chiral effective field theory, Phys. Rev. C **93**, 015501 (2016); **93**, 049902(E) (2016); **95**, 059901(E) (2017).

[15] H. Krebs, E. Epelbaum, and U. G. Meißner, Nuclear axial current operators to fourth order in chiral effective field theory, Ann. Phys. (Amsterdam) **378**, 317 (2017).

[16] P. Gysbers, G. Hagen, J. D. Holt, G. R. Jansen, T. D. Morris, P. Navrátil, T. Papenbrock, S. Quaglioni, A. Schwenk, S. R. Stroberg, and K. A. Wendt, Discrepancy between experimental and theoretical β-decay rates resolved from first principles, Nat. Phys. **15**, 428 (2019).

[17] A. Baroni, G. B. King, and S. Pastore, Electroweak currents from chiral effective field theory, Few-Body Syst. **62**, 114 (2021).

[18] J.-W. Chen, G. Rupak, and M. J. Savage, Nucleon-nucleon effective field theory without pions, Nucl. Phys. **A653**, 386 (1999).

[19] M. Butler and J.-W. Chen, Elastic and inelastic neutrino deuteron scattering in effective field theory, Nucl. Phys. **A675**, 575 (2000).

[20] M. Butler, J.-W. Chen, and P. Vogel, Constraints on two-body axial currents from reactor anti-neutrino deuteron breakup reactions, Phys. Lett. B **549**, 26 (2002).

[21] A. Baroni, L. Girlanda, A. Kievsky, L. E. Marcucci, R. Schiavilla, and M. Viviani, Tritium β-decay in chiral effective field theory, Phys. Rev. C **94**, 024003 (2016); **95**, 059902(E) (2017).

[22] Y.-L. Li, Y.-L. Ma, and M. Rho, Nuclear axial currents from scale-chiral effective field theory, Chin. Phys. C **42**, 094102 (2018).

[23] A. Baroni *et al.*, Local chiral interactions, the tritium Gamow-Teller matrix element, and the three-nucleon contact term, Phys. Rev. C **98**, 044003 (2018).

[24] D. B. Kaplan, M. J. Savage, and M. B. Wise, A New expansion for nucleon-nucleon interactions, Phys. Lett. B **424**, 390 (1998).

[25] D. B. Kaplan, M. J. Savage, and M. B. Wise, Two nucleon systems from effective field theory, Nucl. Phys. **B534**, 329 (1998).
[26] B. Grinstein and I. Z. Rothstein, Effective field theory and matching in nonrelativistic gauge theories, Phys. Rev. D **57**, 78 (1998).
[27] M. E. Luke and M. J. Savage, Power counting in dimensionally regularized NRQCD, Phys. Rev. D **57**, 413 (1998).
[28] A. Parreño, P. E. Shanahan, M. L. Wagman, F. Winter, E. Chang, W. Detmold, and M. Illa (NPLQCD Collaboration), Axial charge of the triton from lattice QCD, Phys. Rev. D **103**, 074511 (2021).
[29] M. J. Dolinski, A. W. Poon, and W. Rodejohann, Neutrinoless double-beta decay: Status and prospects, Annu. Rev. Nucl. Part. Sci. **69**, 219 (2019).
[30] M. J. Savage, Pionic matrix elements in neutrinoless double-beta decay, Phys. Rev. C **59**, 2293 (1999).
[31] P. E. Shanahan, B. C. Tiburzi, M. L. Wagman, F. Winter, E. Chang, Z. Davoudi, W. Detmold, K. Orginos, and M. J. Savage, Isotensor Axial Polarizability and Lattice QCD Input for Nuclear Double-β Decay Phenomenology, Phys. Rev. Lett. **119**, 062003 (2017).
[32] B. C. Tiburzi, M. L. Wagman, F. Winter, E. Chang, Z. Davoudi, W. Detmold, K. Orginos, M. J. Savage, and P. E. Shanahan, Double-β decay matrix elements from lattice quantum chromodynamics, Phys. Rev. D **96**, 054505 (2017).
[33] V. Cirigliano, W. Dekens, J. De Vries, M. L. Graesser, E. Mereghetti, S. Pastore, and U. Van Kolck, New Leading Contribution to Neutrinoless Double-β Decay, Phys. Rev. Lett. **120**, 202001 (2018).
[34] V. Cirigliano, W. Dekens, J. De Vries, M. L. Graesser, E. Mereghetti, S. Pastore, M. Piarulli, U. Van Kolck, and R. B. Wiringa, Renormalized approach to neutrinoless double- β decay, Phys. Rev. C **100**, 055504 (2019).
[35] H. Monge-Camacho, E. Berkowitz, D. Brantley, C. C. Chang, M. A. Clark, A. Gambhir, N. Garrón, B. Joó, T. Kurth, A. Nicholson, E. Rinaldi, B. Tiburzi, P. Vranas, and A. Walker-Loud, Short range operator contributions to $0\nu\beta\beta$ decay from LQCD, Proc. Sci. LATTICE2018 (**2019**) 263.
[36] Z. Davoudi and S. V. Kadam, Extraction of low-energy constants of single- and double-β decays from lattice QCD: A sensitivity analysis, Phys. Rev. D **105**, 094502 (2022).
[37] V. Cirigliano, Z. Davoudi, W. Dekens, J. de Vries, J. Engel, X. Feng, J. Gehrlein, M. L. Graesser, L. Gráf, H. Hergert, L. Jin, E. Mereghetti, A. Nicholson, S. Pastore, M. J. Ramsey-Musolf, R. Ruiz, M. Spinrath, U. van Kolck, and A. Walker-Loud, Neutrinoless double-beta decay: A roadmap for matching theory to experiment, arXiv: 2203.12169.
[38] A. S. Kronfeld *et al.* (USQCD Collaboration), Lattice QCD and particle physics, arXiv:2207.07641.
[39] W. Detmold, W. I. Jay, D. J. Murphy, P. R. Oare, and P. E. Shanahan, Neutrinoless double beta decay from lattice QCD: The short-distance $\pi^- \to \pi^+ e^- e^-$ amplitude, arXiv: 2208.05322.
[40] V. Cirigliano *et al.*, Towards precise and accurate calculations of neutrinoless double-beta decay, J. Phys. G **49**, 120502 (2022).
[41] R. Brower, S. Chandrasekharan, and U. J. Wiese, QCD as a quantum link model, Phys. Rev. D **60**, 094502 (1999).
[42] T. Byrnes and Y. Yamamoto, Simulating lattice gauge theories on a quantum computer, Phys. Rev. A **73**, 022328 (2006).
[43] E. Zohar and B. Reznik, Confinement and Lattice QED Electric Flux-Tubes Simulated with Ultracold Atoms, Phys. Rev. Lett. **107**, 275301 (2011).
[44] E. Zohar, J. I. Cirac, and B. Reznik, Simulating Compact Quantum Electrodynamics with Ultracold Atoms: Probing Confinement and Nonperturbative Effects, Phys. Rev. Lett. **109**, 125302 (2012).
[45] L. Tagliacozzo, A. Celi, A. Zamora, and M. Lewenstein, Optical abelian lattice gauge theories, Ann. Phys. (Amsterdam) **330**, 160 (2013).
[46] D. Banerjee, M. Bögli, M. Dalmonte, E. Rico, P. Stebler, U. J. Wiese, and P. Zoller, Atomic Quantum Simulation of U(N) and SU(N) Non-Abelian Lattice Gauge Theories, Phys. Rev. Lett. **110**, 125303 (2013).
[47] L. Tagliacozzo, A. Celi, P. Orland, and M. Lewenstein, Simulations of non-Abelian gauge theories with optical lattices, Nat. Commun. **4**, 2615 (2013).
[48] E. Zohar, J. I. Cirac, and B. Reznik, Cold-Atom Quantum Simulator for SU(2) Yang-Mills Lattice Gauge Theory, Phys. Rev. Lett. **110**, 125304 (2013).
[49] E. Zohar, J. I. Cirac, and B. Reznik, Simulating $(2+1)$-Dimensional Lattice QED with Dynamical Matter Using Ultracold Atoms, Phys. Rev. Lett. **110**, 055302 (2013).
[50] D. Banerjee, M. Bögli, M. Dalmonte, E. Rico, P. Stebler, U.-J. Wiese, and P. Zoller, Atomic Quantum Simulation of $\mathbf{U}(N)$ and $\mathrm{SU}(N)$ Non-Abelian Lattice Gauge Theories, Phys. Rev. Lett. **110**, 125303 (2013).
[51] U.-J. Wiese, Ultracold quantum gases and lattice systems: Quantum simulation of lattice gauge theories, Ann. Phys. (Amsterdam) **525**, 777 (2013).
[52] P. Hauke, D. Marcos, M. Dalmonte, and P. Zoller, Quantum Simulation of a Lattice Schwinger Model in a Chain of Trapped Ions, Phys. Rev. X **3**, 041018 (2013).
[53] D. Marcos, P. Widmer, E. Rico, M. Hafezi, P. Rabl, U. J. Wiese, and P. Zoller, Two-dimensional lattice gauge theories with superconducting quantum circuits, Ann. Phys. (Amsterdam) **351**, 634 (2014).
[54] Y. Kuno, K. Kasamatsu, Y. Takahashi, I. Ichinose, and T. Matsui, Real-time dynamics and proposal for feasible experiments of lattice gauge–Higgs model simulated by cold atoms, New J. Phys. **17**, 063005 (2015).
[55] A. Bazavov, Y. Meurice, S.-W. Tsai, J. Unmuth-Yockey, and J. Zhang, Gauge-invariant implementation of the Abelian Higgs model on optical lattices, Phys. Rev. D **92**, 076003 (2015).
[56] V. Kasper, F. Hebenstreit, M. Oberthaler, and J. Berges, Schwinger pair production with ultracold atoms, Phys. Lett. B **760**, 742 (2016).
[57] G. K. Brennen, G. Pupillo, E. Rico, T. M. Stace, and D. Vodola, Loops and Strings in a Superconducting Lattice Gauge Simulator, Phys. Rev. Lett. **117**, 240504 (2016).
[58] Y. Kuno, S. Sakane, K. Kasamatsu, I. Ichinose, and T. Matsui, Atomic quantum simulation of a three-dimensional U(1) gauge-Higgs model, Phys. Rev. A **94**, 063641 (2016).

[59] E. A. Martinez, C. A. Muschik, P. Schindler, D. Nigg, A. Erhard, M. Heyl, P. Hauke, M. Dalmonte, T. Monz, P. Zoller, and R. Blatt, Real-time dynamics of lattice gauge theories with a few-qubit quantum computer, Nature (London) **534**, 516 (2016).

[60] E. Zohar, A. Farace, B. Reznik, and J. I. Cirac, Digital lattice gauge theories, Phys. Rev. A **95**, 023604 (2017).

[61] V. Kasper, F. Hebenstreit, F. Jendrzejewski, M. K. Oberthaler, and J. Berges, Implementing quantum electrodynamics with ultracold atomic systems, New J. Phys. **19**, 023030 (2017).

[62] C. Muschik, M. Heyl, E. Martinez, T. Monz, P. Schindler, B. Vogell, M. Dalmonte, P. Hauke, R. Blatt, and P. Zoller, U(1) Wilson lattice gauge theories in digital quantum simulators, New J. Phys. **19**, 103020 (2017).

[63] D. González-Cuadra, E. Zohar, and J. I. Cirac, Quantum simulation of the abelian-Higgs lattice gauge theory with ultracold atoms, New J. Phys. **19**, 063038 (2017).

[64] M. C. Bañuls, K. Cichy, J. I. Cirac, K. Jansen, and S. Kühn, Efficient Basis Formulation for $1+1$ Dimensional SU(2) Lattice Gauge Theory: Spectral Calculations with Matrix Product States, Phys. Rev. X **7**, 041046 (2017).

[65] E. F. Dumitrescu, A. J. McCaskey, G. Hagen, G. R. Jansen, T. D. Morris, T. Papenbrock, R. C. Pooser, D. J. Dean, and P. Lougovski, Cloud Quantum Computing of an Atomic Nucleus, Phys. Rev. Lett. **120**, 210501 (2018).

[66] N. Klco, E. F. Dumitrescu, A. J. McCaskey, T. D. Morris, R. C. Pooser, M. Sanz, E. Solano, P. Lougovski, and M. J. Savage, Quantum-classical computation of Schwinger model dynamics using quantum computers, Phys. Rev. A **98**, 032331 (2018).

[67] D. B. Kaplan and J. R. Stryker, Gauss's law, duality, and the Hamiltonian formulation of U(1) lattice gauge theory, Phys. Rev. D **102**, 094515 (2020).

[68] C. Kokail, C. Maier, R. van Bijnen, T. Brydges, M. K. Joshi, P. Jurcevic, C. A. Muschik, P. Silvi, R. Blatt, C. F. Roos, and P. Zoller, Self-verifying variational quantum simulation of lattice models, Nature (London) **569**, 355 (2019).

[69] H.-H. Lu, N. Klco, J. M. Lukens, T. D. Morris, A. Bansal, A. Ekström, G. Hagen, T. Papenbrock, A. M. Weiner, M. J. Savage, and P. Lougovski, Simulations of subatomic many-body physics on a quantum frequency processor, Phys. Rev. A **100**, 012320 (2019).

[70] K. Yeter-Aydeniz, E. F. Dumitrescu, A. J. McCaskey, R. S. Bennink, R. C. Pooser, and G. Siopsis, Scalar quantum field theories as a benchmark for near-term quantum computers, Phys. Rev. A **99**, 032306 (2019).

[71] J. R. Stryker, Oracles for Gauss's law on digital quantum computers, Phys. Rev. A **99**, 042301 (2019).

[72] E. Gustafson, Y. Meurice, and J. Unmuth-Yockey, Quantum simulation of scattering in the quantum Ising model, Phys. Rev. D **99**, 094503 (2019).

[73] J. Arrington *et al.*, Opportunities for nuclear physics & quantum information science, in *Intersections Between Nuclear Physics and Quantum Information*, edited by I. C. Cloët and M. R. Dietrich (2019).

[74] C. W. Bauer, W. A. de Jong, B. Nachman, and D. Provasoli, Quantum Algorithm for High Energy Physics Simulations, Phys. Rev. Lett. **126**, 062001 (2021).

[75] O. Shehab, K. A. Landsman, Y. Nam, D. Zhu, N. M. Linke, M. J. Keesan, R. C. Pooser, and C. R. Monroe, Toward convergence of effective field theory simulations on digital quantum computers, Phys. Rev. A **100**, 062319 (2019).

[76] N. Klco and M. J. Savage, Minimally entangled state preparation of localized wave functions on quantum computers, Phys. Rev. A **102**, 012612 (2020).

[77] A. Alexandru, P. F. Bedaque, S. Harmalkar, H. Lamm, S. Lawrence, and N. C. Warrington (NuQS Collaboration), Gluon field digitization for quantum computers, Phys. Rev. D **100**, 114501 (2019).

[78] Z. Davoudi, M. Hafezi, C. Monroe, G. Pagano, A. Seif, and A. Shaw, toward analog quantum simulations of lattice gauge theories with trapped ions, Phys. Rev. Res. **2**, 023015 (2020).

[79] A. Avkhadiev, P. E. Shanahan, and R. D. Young, Accelerating Lattice Quantum Field Theory Calculations via Interpolator Optimization Using Noisy Intermediate-Scale Quantum Computing, Phys. Rev. Lett. **124**, 080501 (2020).

[80] N. Klco, J. R. Stryker, and M. J. Savage, SU(2) non-Abelian gauge field theory in one dimension on digital quantum computers, Phys. Rev. D **101**, 074512 (2020).

[81] G. Magnifico, M. Dalmonte, P. Facchi, S. Pascazio, F. V. Pepe, and E. Ercolessi, Real time dynamics and confinement in the $\mathbb{Z}_n$ Schwinger-Weyl lattice model for $1+1$ QED, Quantum **4**, 281 (2020).

[82] E. Gustafson, P. Dreher, Z. Hang, and Y. Meurice, Indexed improvements for real-time trotter evolution of a $(1+1)$ field theory using NISQ quantum computers, Quantum Sci. Technol. **6**, 045020 (2021).

[83] M. C. Bañuls, R. Blatt, J. Catani, A. Celi, J. I. Cirac, M. Dalmonte, L. Fallani, K. Jansen, M. Lewenstein, S. Montangero, C. A. Muschik, B. Reznik, E. Rico, L. Tagliacozzo, K. V. Acoleyen, F. Verstraete, U.-J. Wiese, M. Wingate, J. Zakrzewski, and P. Zoller, Simulating lattice gauge theories within quantum technologies, Eur. Phys. J. D **74**, 165 (2020).

[84] N. Klco and M. J. Savage, Systematically localizable operators for quantum simulations of quantum field theories, Phys. Rev. A **102**, 012619 (2020).

[85] C. Mishra, S. Thompson, R. Pooser, and G. Siopsis, Quantum computation of an interacting fermionic model, Quantum Sci. Technol. **5**, 035010 (2020).

[86] D. Luo, J. Shen, M. Highman, B. K. Clark, B. DeMarco, A. X. El-Khadra, and B. Gadway, Framework for simulating gauge theories with dipolar spin systems, Phys. Rev. A **102**, 032617 (2020).

[87] D. E. Kharzeev and Y. Kikuchi, Real-time chiral dynamics from a digital quantum simulation, Phys. Rev. Res. **2**, 023342 (2020).

[88] N. Mueller, A. Tarasov, and R. Venugopalan, Computing real time correlation functions on a hybrid classical/quantum computer, Nucl. Phys. **A1005**, 121889 (2021).

[89] A. F. Shaw, P. Lougovski, J. R. Stryker, and N. Wiebe, Quantum algorithms for simulating the lattice Schwinger model, Quantum **4**, 306 (2020).

[90] T. V. Zache, N. Mueller, J. T. Schneider, F. Jendrzejewski, J. Berges, and P. Hauke, Dynamical Topological Transitions

in the Massive Schwinger Model with a θ Term, Phys. Rev. Lett. **122**, 050403 (2019).
[91] B. Yang, H. Sun, R. Ott, H.-Y. Wang, T. V. Zache, J. C. Halimeh, Z.-S. Yuan, P. Hauke, and J.-W. Pan, Observation of gauge invariance in a 71-site bose-hubbard quantum simulator, Nature (London) **587**, 392 (2020).
[92] Y. Ji, H. Lamm, and S. Zhu (NuQS Collaboration), Gluon field digitization via group space decimation for quantum computers, Phys. Rev. D **102**, 114513 (2020).
[93] J. Bender, P. Emonts, E. Zohar, and J. I. Cirac, Real-time dynamics in $2+1D$ compact QED using complex periodic Gaussian states, Phys. Rev. Res. **2**, 043145 (2020).
[94] J. F. Haase, L. Dellantonio, A. Celi, D. Paulson, A. Kan, K. Jansen, and C. A. Muschik, A resource efficient approach for quantum and classical simulations of gauge theories in particle physics, Quantum **5**, 393 (2021).
[95] J. C. Halimeh, H. Lang, J. Mildenberger, Z. Jiang, and P. Hauke, Gauge-symmetry protection using single-body terms, PRX Quantum **2**, 040311 (2021).
[96] D. Robaina, M. C. Bañuls, and J. I. Cirac, Simulating $2+1D$ Z_3 Lattice Gauge Theory with an Infinite Projected Entangled-Pair State, Phys. Rev. Lett. **126**, 050401 (2021).
[97] K. Yeter-Aydeniz, G. Siopsis, and R. C. Pooser, Scattering in the Ising model with the quantum Lanczos algorithm, New J. Phys. **23**, 043033 (2021).
[98] D. Paulson, L. Dellantonio, J. F. Haase, A. Celi, A. Kan, A. Jena, C. Kokail, R. van Bijnen, K. Jansen, P. Zoller, and C. A. Muschik, toward simulating 2D effects in lattice gauge theories on a quantum computer, PRX Quantum **2**, 030334 (2021).
[99] J. C. Halimeh, V. Kasper, and P. Hauke, Fate of lattice gauge theories under decoherence, arXiv:2009.07848.
[100] M. Van Damme, J. C. Halimeh, and P. Hauke, Gauge-symmetry violation quantum phase transition in lattice gauge theories, arXiv:2010.07338.
[101] J. a. Barata, N. Mueller, A. Tarasov, and R. Venugopalan, Single-particle digitization strategy for quantum computation of a ϕ^4 scalar field theory, Phys. Rev. A **103**, 042410 (2021).
[102] A. Milsted, J. Liu, J. Preskill, and G. Vidal, Collisions of false-vacuum bubble walls in a quantum spin chain, PRX Quantum **3**, 020316 (2022).
[103] V. Kasper, T. V. Zache, F. Jendrzejewski, M. Lewenstein, and E. Zohar, Non-Abelian gauge invariance from dynamical decoupling, Phys. Rev. D **107**, 014506 (2023).
[104] R. Ott, T. V. Zache, F. Jendrzejewski, and J. Berges, Scalable Cold-Atom Quantum Simulator for Two-Dimensional QED, Phys. Rev. Lett. **127**, 130504 (2021).
[105] A. Ciavarella, N. Klco, and M. J. Savage, Trailhead for quantum simulation of SU(3) Yang-Mills lattice gauge theory in the local multiplet basis, Phys. Rev. D **103**, 094501 (2021).
[106] C. W. Bauer, M. Freytsis, and B. Nachman, Simulating Collider Physics on Quantum Computers Using Effective Field Theories, Phys. Rev. Lett. **127**, 212001 (2021).
[107] E. Gustafson, Y. Zhu, P. Dreher, N. M. Linke, and Y. Meurice, Real-time quantum calculations of phase shifts using wave packet time delays, Phys. Rev. D **104**, 054507 (2021).
[108] S. A Rahman, R. Lewis, E. Mendicelli, and S. Powell, SU(2) lattice gauge theory on a quantum annealer, Phys. Rev. D **104**, 034501 (2021).
[109] Y. Y. Atas, J. Zhang, R. Lewis, A. Jahanpour, J. F. Haase, and C. A. Muschik, SU(2) hadrons on a quantum computer via a variational approach, Nat. Commun. **12**, 6499 (2021).
[110] K. Yeter-Aydeniz, S. Bangar, G. Siopsis, and R. C. Pooser, Collective neutrino oscillations on a quantum computer, Quantum Inf. Process. **21**, 84 (2022).
[111] Z. Davoudi, N. M. Linke, and G. Pagano, Toward simulating quantum field theories with controlled phonon-ion dynamics: A hybrid analog-digital approach, Phys. Rev. Res. **3**, 043072 (2021).
[112] A. Kan, L. Funcke, S. Kühn, L. Dellantonio, J. Zhang, J. F. Haase, C. A. Muschik, and K. Jansen, Investigating a $3+1$D topological θ-term in the Hamiltonian formulation of lattice gauge theories for quantum and classical simulations, Phys. Rev. D **104**, 034504 (2021).
[113] J. R. Stryker, Shearing approach to gauge invariant Trotterization, arXiv:2105.11548.
[114] M. Aidelsburger *et al.*, Cold atoms meet lattice gauge theory, Phil. Trans. R. Soc. A **380**, 20210064 (2021).
[115] E. Zohar, Quantum simulation of lattice gauge theories in more than one space dimension—requirements, challenges and methods, Phil. Trans. R. Soc. A **380**, 20210069 (2021).
[116] J. C. Halimeh, H. Lang, and P. Hauke, Gauge protection in non-abelian lattice gauge theories, New J. Phys. **24**, 033015 (2022).
[117] K. Yeter-Aydeniz, E. Moschandreou, and G. Siopsis, Quantum imaginary-time evolution algorithm for quantum field theories with continuous variables, Phys. Rev. A **105**, 012412 (2022).
[118] J. Knaute and P. Hauke, Relativistic meson spectra on ion-trap quantum simulators, Phys. Rev. A **105**, 022616 (2022).
[119] U.-J. Wiese, From quantum link models to D-theory: A resource efficient framework for the quantum simulation and computation of gauge theories, Phil. Trans. R. Soc. A **380**, 20210068 (2021).
[120] Y. Meurice, Theoretical methods to design and test quantum simulators for the compact Abelian Higgs model, Phys. Rev. D **104**, 094513 (2021).
[121] N. Mueller, T. V. Zache, and R. Ott, Thermalization of Gauge Theories from their Entanglement Spectrum, Phys. Rev. Lett. **129**, 011601 (2022).
[122] H. Riechert, J. C. Halimeh, V. Kasper, L. Bretheau, E. Zohar, P. Hauke, and F. Jendrzejewski, Engineering a U(1) lattice gauge theory in classical electric circuits, Phys. Rev. B **105**, 205141 (2022).
[123] J. C. Halimeh, L. Homeier, C. Schweizer, M. Aidelsburger, P. Hauke, and F. Grusdt, Stabilizing lattice gauge theories through simplified local pseudogenerators, Phys. Rev. Res. **4**, 033120 (2022).
[124] J. Zhang, R. Ferguson, S. Kühn, J. F. Haase, C. M. Wilson, K. Jansen, and C. A. Muschik, Simulating gauge theories with variational quantum eigensolvers in superconducting microwave cavities, arXiv:2108.08248.
[125] M. S. Alam, S. Hadfield, H. Lamm, and A. C. Y. Li (SQMS Collaboration), Primitive quantum gates for dihedral gauge theories, Phys. Rev. D **105**, 114501 (2022).

[126] P. Deliyannis, M. Freytsis, B. Nachman, and C. W. Bauer, Practical considerations for the preparation of multivariate Gaussian states on quantum computers, arXiv:2109.10918.
[127] M. A. Perlin, D. Barberena, M. Mamaev, B. Sundar, R. J. Lewis-Swan, and A. M. Rey, Engineering infinite-range SU(n) interactions with spin-orbit-coupled fermions in an optical lattice, Phys. Rev. A **105**, 023326 (2022).
[128] L. Funcke, T. Hartung, K. Jansen, S. Kühn, M. Schneider, P. Stornati, and X. Wang, Toward quantum simulations in particle physics and beyond on noisy intermediate-scale quantum devices, Phil. Trans. R. Soc. A **380**, 20210062 (2021).
[129] E. Gustafson, B. Holzman, J. Kowalkowski, H. Lamm, A. C. Y. Li, G. Perdue, S. Boixo, S. Isakov, O. Martin, R. Thomson, C. V. Heidweiller, J. Beall, M. Ganahl, G. Vidal, and E. Peters, Large scale multi-node simulations of $\mathbb{Z}_2$ gauge theory quantum circuits using Google Cloud Platform, in *IEEE/ACM Second International Workshop on Quantum Computing Software* (2021), arXiv:2110.07482.
[130] M. Van Damme, J. Mildenberger, F. Grusdt, P. Hauke, and J. C. Halimeh, Suppressing nonperturbative gauge errors in the thermodynamic limit using local pseudogenerators, arXiv:2110.08041.
[131] S. Thompson and G. Siopsis, Quantum computation of phase transition in the massive Schwinger model, Quantum Sci. Technol. **7**, 035001 (2022).
[132] A. Kan, L. Funcke, S. Kühn, L. Dellantonio, J. Zhang, J. F. Haase, C. A. Muschik, and K. Jansen, $3+1$D θ-term on the lattice from the Hamiltonian perspective, Proc. Sci. LATTICE2021 (**2022**) 112.
[133] S. Ashkenazi and E. Zohar, Duality as a feasible physical transformation for quantum simulation, Phys. Rev. A **105**, 022431 (2022).
[134] C. Alexandrou, L. Funcke, T. Hartung, K. Jansen, S. Kühn, G. Polykratis, P. Stornati, X. Wang, and T. Weber, Investigating the variance increase of readout error mitigation through classical bit-flip correction on IBM and Rigetti quantum computers, Proc. Sci. LATTICE2021 (**2022**) 243.
[135] C. W. Bauer and D. M. Grabowska, Efficient representation for simulating U(1) gauge theories on digital quantum computers at all values of the coupling, Phys. Rev. D **107**, L031503 (2023).
[136] X. Wang, X. Feng, L. Funcke, T. Hartung, K. Jansen, S. Kühn, G. Polykratis, and P. Stornati, Model-independent error mitigation in parametric quantum circuits and depolarizing projection of quantum noise, Proc. Sci. LATTICE2021 (**2022**) 603.
[137] G. Iannelli and K. Jansen, Noisy Bayesian optimization for variational quantum eigensolvers, Proc. Sci. LATTICE2021 (**2022**) 251.
[138] A. N. Ciavarella and I. A. Chernyshev, Preparation of the SU(3) lattice Yang-Mills vacuum with variational quantum methods, Phys. Rev. D **105**, 074504 (2022).
[139] N. H. Nguyen, M. C. Tran, Y. Zhu, A. M. Green, C. H. Alderete, Z. Davoudi, and N. M. Linke, Digital quantum simulation of the Schwinger model and symmetry protection with trapped ions, PRX Quantum **3**, 020324 (2022).
[140] K. Yeter-Aydeniz, Z. Parks, A. Nair, E. Gustafson, A. F. Kemper, R. C. Pooser, Y. Meurice, and P. Dreher, Measuring qubit stability in a gate-based NISQ hardware processor, Quantum Inf Process **22**, 96 (2023).
[141] T. Hartung, T. Jakobs, K. Jansen, J. Ostmeyer, and C. Urbach, Digitising SU(2) gauge fields and the freezing transition, Eur. Phys. J. C **82**, 237 (2022).
[142] M. Illa and M. J. Savage, Basic elements for simulations of standard model physics with quantum annealers: Multigrid and clock states, Phys. Rev. A **106**, 052605 (2022).
[143] Y. Ji, H. Lamm, and S. Zhu, Gluon digitization via character expansion for quantum computers, arXiv:2203.02330.
[144] M. Carena, H. Lamm, Y.-Y. Li, and W. Liu, Improved Hamiltonians for Quantum Simulations of Gauge Theories, Phys. Rev. Lett. **129**, 051601 (2022).
[145] J. C. Halimeh, L. Barbiero, P. Hauke, F. Grusdt, and A. Bohrdt, Robust quantum many-body scars in lattice gauge theories, arXiv:2203.08828.
[146] J. Mildenberger, W. Mruczkiewicz, J. C. Halimeh, Z. Jiang, and P. Hauke, Probing confinement in a $\mathbb{Z}_2$ lattice gauge theory on a quantum computer, arXiv:2203.08905.
[147] P. Deliyannis, J. Sud, D. Chamaki, Z. Webb-Mack, C. W. Bauer, and B. Nachman, Improving quantum simulation efficiency of final state radiation with dynamic quantum circuits, Phys. Rev. D **106**, 036007 (2022).
[148] A. Ciavarella, N. Klco, and M. J. Savage, Some conceptual aspects of operator design for quantum simulations of non-abelian lattice gauge theories, arXiv:2203.11988.
[149] S. Caspar and H. Singh, From Asymptotic Freedom to θ Vacua: Qubit Embeddings of the O(3) Nonlinear σ Model, Phys. Rev. Lett. **129**, 022003 (2022).
[150] C. W. Bauer *et al.*, Quantum simulation for high energy physics, arXiv:2204.03381.
[151] J. C. Halimeh, I. P. McCulloch, B. Yang, and P. Hauke, Tuning the topological θ-angle in cold-atom quantum simulators of gauge theories, PRX Quantum **3**, 040316 (2022).
[152] J. C. Halimeh and P. Hauke, Stabilizing gauge theories in quantum simulators: A brief review, arXiv:2204.13709.
[153] I. Raychowdhury, Z. Davoudi, and A. Shaw, Exploring different formulations of non-abelian lattice gauge theories for Hamiltonian simulation, Proc. Sci. LATTICE2021 (**2022**) 277.
[154] P. Dreher, E. Gustafson, Y. Zhu, N. M. Linke, and Y. Meurice, Real-time quantum calculations of phase shifts On NISQ hardware platforms using wavepacket time delay, Proc. Sci. LATTICE2021 (**2022**) 464.
[155] S. A Rahman, R. Lewis, E. Mendicelli, and S. Powell, Self-mitigating Trotter circuits for SU(2) lattice gauge theory on a quantum computer, Phys. Rev. D **106**, 074502 (2022).
[156] T. Greenberg, G. Pardo, A. Fortinsky, and E. Zohar, Resource-efficient quantum simulation of lattice gauge theories in arbitrary dimensions: Solving for Gauss' law and fermion elimination, arXiv:2206.00685.
[157] C. Tüysüz, G. Clemente, A. Crippa, T. Hartung, S. Kühn, and K. Jansen, Classical splitting of parametrized quantum circuits, arXiv:2206.09641.
[158] R. C. Farrell, I. A. Chernyshev, S. J. M. Powell, N. A. Zemlevskiy, M. Illa, and M. J. Savage, preceding paper, Preparations for quantum simulations of quantum chromodynamics in $1+1$ dimensions. (I). Axial gauge, Phys. Rev. D **107**, 054512 (2023).

[159] Y. Y. Atas, J. F. Haase, J. Zhang, V. Wei, S. M. L. Pfaendler, R. Lewis, and C. A. Muschik, Real-time evolution of SU(3) hadrons on a quantum computer, arXiv:2207.03473.
[160] J. Bringewatt and Z. Davoudi, Parallelization techniques for quantum simulation of fermionic systems, arXiv:2207.12470.
[161] D. M. Grabowska, C. Kane, B. Nachman, and C. W. Bauer, Overcoming exponential scaling with system size in Trotter-Suzuki implementations of constrained Hamiltonians: $2+1$ U(1) lattice gauge theories, arXiv:2208.03333.
[162] M. Asaduzzaman, S. Catterall, G. C. Toga, Y. Meurice, and R. Sakai, Quantum simulation of the N flavor Gross-Neveu model, Phys. Rev. D **106**, 114515 (2022).
[163] M. Carena, E. J. Gustafson, H. Lamm, Y.-Y. Li, and W. Liu, Gauge theory couplings on anisotropic lattices, Phys. Rev. D **106**, 114504 (2022).
[164] E. J. Gustafson, H. Lamm, F. Lovelace, and D. Musk, Primitive quantum gates for an SU(2) discrete subgroup: BT, Phys. Rev. D **106**, 114501 (2022).
[165] Z. Davoudi, N. Mueller, and C. Powers, Toward quantum computing phase diagrams of gauge theories with thermal pure quantum states, arXiv:2208.13112.
[166] A. Avkhadiev, P. E. Shanahan, and R. D. Young, Strategies for quantum-optimized construction of interpolating operators in classical simulations of lattice quantum field theories, arXiv:2209.01209.
[167] W. Jang, K. Terashi, M. Saito, C. W. Bauer, B. Nachman, Y. Iiyama, R. Okubo, and R. Sawada, Initial-state dependent optimization of controlled gate operations with quantum computer, Quantum **6**, 798 (2022).
[168] A. Ciavarella, Algorithm for quantum computation of particle decays, Phys. Rev. D **102**, 094505 (2020).
[169] P. Jordan and E. P. Wigner, About the Pauli exclusion principle, Z. Phys. **47**, 631 (1928).
[170] IBM Quantum, https://quantum-computing.ibm.com/ (2022).
[171] E. C. G. Sudarshan and R. e. Marshak, Chirality invariance and the universal Fermi interaction, Phys. Rev. **109**, 1860 (1958).
[172] E. Tiesinga, P. J. Mohr, D. B. Newell, and B. N. Taylor, CODATA recommended values of the fundamental physical constants: 2018, Rev. Mod. Phys. **93**, 025010 (2021).
[173] J. B. Kogut and L. Susskind, Hamiltonian formulation of Wilson's lattice gauge theories, Phys. Rev. D **11**, 395 (1975).
[174] T. Banks, L. Susskind, and J. B. Kogut, Strong coupling calculations of lattice gauge theories: $(1+1)$-dimensional exercises, Phys. Rev. D **13**, 1043 (1976).
[175] S. Weinberg, Baryon and Lepton Nonconserving Processes, Phys. Rev. Lett. **43**, 1566 (1979).
[176] Quantinuum, https://www.quantinuum.com/ (2022).
[177] Quantinuum, Quantinuum System Model H1 Emulator Product Data Sheet, Version 5.00 (2022).
[178] A. Peruzzo, J. McClean, P. Shadbolt, M.-H. Yung, X.-Q. Zhou, P. J. Love, A. Aspuru-Guzik, and J. L. O'Brien, A variational eigenvalue solver on a photonic quantum processor, Nat. Commun. **5**, 4213 (2014).
[179] M. Treinish *et al.*, Qiskit/qiskit: Qiskit 0.36.2 (2022).
[180] S. Ghosh, R. M. Soni, and S. P. Trivedi, On the entanglement entropy for gauge theories, J. High Energy Phys. 09 (2015) 069.
[181] R. M. Soni and S. P. Trivedi, Aspects of entanglement entropy for gauge theories, J. High Energy Phys. 01 (2016) 136.
[182] V. Panizza, R. C. de Almeida, and P. Hauke, Entanglement witnessing for lattice gauge theories, J. High Energy Phys. 09 (2022) 196.
[183] M. Rigobello, S. Notarnicola, G. Magnifico, and S. Montangero, Entanglement generation in $(1+1)$D QED scattering processes, Phys. Rev. D **104**, 114501 (2021).
[184] E. Pelofske, A. Bärtschi, and S. Eidenbenz, Quantum volume in practice: What users can expect from NISQ devices, IEEE Trans. Quantum Eng. **3**, 1 (2022).
[185] H. Kamakari, S.-N. Sun, M. Motta, and A. J. Minnich, Digital quantum simulation of open quantum systems using quantum imaginary time evolution, PRX Quantum **3**, 010320 (2022).
[186] J. Hubisz, B. Sambasivam, and J. Unmuth-Yockey, Quantum algorithms for open lattice field theory, Phys. Rev. A **104**, 052420 (2021).
[187] F. Turro, A. Roggero, V. Amitrano, P. Luchi, K. A. Wendt, J. L. DuBois, S. Quaglioni, and F. Pederiva, Imaginary-time propagation on a quantum chip, Phys. Rev. A **105**, 022440 (2022).
[188] Wolfram Research, Inc., *Mathematica*, Version 12.3.10 (2022), Champaign, IL.
[189] G. Van Rossum and F. L. Drake, *Python 3 Reference Manual* (CreateSpace, Scotts Valley, CA, 2009).
[190] J. D. Hunter, Matplotlib: A 2D graphics environment, Comput. Sci. Eng. **9**, 90 (2007).
[191] J. Bezanson, A. Edelman, S. Karpinski, and V. B. Shah, Julia: A fresh approach to numerical computing, SIAM Rev. **59**, 65 (2017).
[192] F. Pérez and B. E. Granger, IPython: A system for interactive scientific computing, Comput. Sci. Eng. **9**, 21 (2007).
[193] Anaconda Inc., Anaconda Software Distribution, Vers. 2-2.4.0 (2020).
[194] C. Developers, Cirq (2022), See full list of authors on Github: https://github.com/quantumlib/Cirq/graphs/contributors.
[195] S. Sivarajah, S. Dilkes, A. Cowtan, W. Simmons, A. Edgington, and R. Duncan, t|ket⟩: A retargetable compiler for NISQ devices, Quantum Sci. Technol. **6**, 014003 (2020).
[196] R. L. Workman *et al.* (Particle Data Group), Review of particle physics, Prog. Theor. Exp. Phys. **2022**, 083C01 (2022).
[197] M. Lüscher, Volume dependence of the energy spectrum in massive quantum field theories. 1. Stable particle states, Commun. Math. Phys. **104**, 177 (1986).
[198] M. Lüscher, Volume dependence of the energy spectrum in massive quantum field theories. 2. Scattering states, Commun. Math. Phys. **105**, 153 (1986).
[199] M. Lüscher, Two particle states on a torus and their relation to the scattering matrix, Nucl. Phys. **B354**, 531 (1991).

[200] L. Lellouch and M. Lüscher, Weak transition matrix elements from finite volume correlation functions, Commun. Math. Phys. **219**, 31 (2001).
[201] W. Detmold and M. J. Savage, Electroweak matrix elements in the two nucleon sector from lattice QCD, Nucl. Phys. **A743**, 170 (2004).
[202] N. H. Christ, C. Kim, and T. Yamazaki, Finite volume corrections to the two-particle decay of states with nonzero momentum, Phys. Rev. D **72**, 114506 (2005).
[203] C. h. Kim, C. T. Sachrajda, and S. R. Sharpe, Finite-volume effects for two-hadron states in moving frames, Nucl. Phys. **B727**, 218 (2005).
[204] M. T. Hansen and S. R. Sharpe, Multiple-channel generalization of Lellouch-Lüscher formula, Phys. Rev. D **86**, 016007 (2012).
[205] H. B. Meyer, Lattice QCD and the Timelike Pion Form Factor, Phys. Rev. Lett. **107**, 072002 (2011).
[206] R. A. Briceño and Z. Davoudi, Moving multichannel systems in a finite volume with application to proton-proton fusion, Phys. Rev. D **88**, 094507 (2013).
[207] X. Feng, S. Aoki, S. Hashimoto, and T. Kaneko, Timelike pion form factor in lattice QCD, Phys. Rev. D **91**, 054504 (2015).
[208] H. B. Meyer, Photodisintegration of a bound state on the torus, arXiv:1202.6675.
[209] V. Bernard, D. Hoja, U. G. Meißner, and A. Rusetsky, Matrix elements of unstable states, J. High Energy Phys. 09 (2012) 023.
[210] A. Agadjanov, V. Bernard, U. G. Meißner, and A. Rusetsky, A framework for the calculation of the $\Delta N\gamma^*$ transition form factors on the lattice, Nucl. Phys. **B886**, 1199 (2014).
[211] R. A. Briceño, M. T. Hansen, and A. Walker-Loud, Multichannel $1 \to 2$ transition amplitudes in a finite volume, Phys. Rev. D **91**, 034501 (2015).
[212] R. A. Briceño and M. T. Hansen, Multichannel $0 \to 2$ and $1 \to 2$ transition amplitudes for arbitrary spin particles in a finite volume, Phys. Rev. D **92**, 074509 (2015).
[213] R. A. Briceño and M. T. Hansen, Relativistic, model-independent, multichannel $2 \to 2$ transition amplitudes in a finite volume, Phys. Rev. D **94**, 013008 (2016).
[214] R. A. Briceño, Z. Davoudi, M. T. Hansen, M. R. Schindler, and A. Baroni, Long-range electroweak amplitudes of single hadrons from Euclidean finite-volume correlation functions, Phys. Rev. D **101**, 014509 (2020).
[215] R. A. Briceño, A. W. Jackura, F. G. Ortega-Gama, and K. H. Sherman, On-shell representations of two-body transition amplitudes: Single external current, Phys. Rev. D **103**, 114512 (2021).
[216] S. R. Beane, P. F. Bedaque, A. Parreño, and M. J. Savage, Two nucleons on a lattice, Phys. Lett. B **585**, 106 (2004).
[217] S. R. Beane, W. Detmold, and M. J. Savage, n-boson energies at finite volume and three-boson interactions, Phys. Rev. D **76**, 074507 (2007).
[218] S. R. Beane, W. Detmold, T. C. Luu, K. Orginos, M. J. Savage, and A. Torok, Multi-Pion Systems in Lattice QCD and the Three-Pion Interaction, Phys. Rev. Lett. **100**, 082004 (2008).
[219] T. Luu, M. J. Savage, A. Schwenk, and J. P. Vary, Nucleon-nucleon scattering in a harmonic potential, Phys. Rev. C **82**, 034003 (2010).
[220] T. Luu and M. J. Savage, Extracting scattering phase-shifts in higher partial-waves from lattice QCD calculations, Phys. Rev. D **83**, 114508 (2011).
[221] Z. Davoudi and M. J. Savage, Improving the volume dependence of two-body binding energies calculated with lattice QCD, Phys. Rev. D **84**, 114502 (2011).
[222] R. A. Briceño and Z. Davoudi, Three-particle scattering amplitudes from a finite volume formalism, Phys. Rev. D **87**, 094507 (2013).
[223] R. A. Briceño, Z. Davoudi, and T. C. Luu, Two-nucleon systems in a finite volume: (I) Quantization conditions, Phys. Rev. D **88**, 034502 (2013).
[224] R. A. Briceño, Z. Davoudi, T. Luu, and M. J. Savage, Two-nucleon systems in a finite volume. II. ${}^3S_1 - {}^3D_1$ coupled channels and the deuteron, Phys. Rev. D **88**, 114507 (2013).
[225] R. A. Briceño, Z. Davoudi, T. C. Luu, and M. J. Savage, Two-baryon systems with twisted boundary conditions, Phys. Rev. D **89**, 074509 (2014).
[226] R. A. Briceño, Two-particle multichannel systems in a finite volume with arbitrary spin, Phys. Rev. D **89**, 074507 (2014).
[227] D. M. Grabowska and M. T. Hansen, Analytic expansions of two- and three-particle excited-state energies, Proc. Sci. LATTICE2021 (**2022**) 203.
[228] L. Maiani and M. Testa, Final state interactions from Euclidean correlation functions, Phys. Lett. B **245**, 585 (1990).
[229] R. A. Briceño, J. V. Guerrero, M. T. Hansen, and A. M. Sturzu, Role of boundary conditions in quantum computations of scattering observables, Phys. Rev. D **103**, 014506 (2020).
[230] K. Urbanowski, True quantum face of the "exponential" decay law, Eur. Phys. J. D **71**, 118 (2017).
[231] F. Giacosa, Time evolution of an unstable quantum system, Acta Phys. Pol. B **48**, 1831 (2017).
[232] O. Katz, L. Feng, A. Risinger, C. Monroe, and M. Cetina, Demonstration of three- and four-body interactions between trapped-ion spins, arXiv:2209.05691.
[233] O. Katz, M. Cetina, and C. Monroe, Programmable N-body interactions with trapped ions, arXiv:2207.10550.
[234] B. Andrade, Z. Davoudi, T. Graß, M. Hafezi, G. Pagano, and A. Seif, Engineering an effective three-spin Hamiltonian in trapped-ion systems for applications in quantum simulation, Quantum Sci. Technol. **7**, 034001 (2022).
[235] Quantinuum, System Model H1 Product Data Sheet, Version 5.00 (2022).

Correction: Minor errors in Eqs. (E2) and (E3) have been fixed.